

# Instrumentation of an Opto-Digital Confocal Microscope and Development of a DMD-Based Imaging Setup

by

Berk Zengin

A Dissertation Submitted to the  
Graduate School of Sciences and Engineering  
in Partial Fulfillment of the Requirements for  
the Degree of

Master of Science

in

Physics



August, 2018

Koc University  
Graduate School of Sciences and Engineering

This is to certify that I have examined this copy of a master's thesis by

Berk Zengin

and have found that it is complete and satisfactory in all respects,  
and that any and all revisions required by the  
examining committee have been made.

Committee Members:

Alper Kiraz, Ph. D.(Advisor)

Aşkın Kocabaş, Ph. D.

Oğuzhan Gürlü, Ph. D.

Date:

10.08.2018

To my family and all beloved friends

## ABSTRACT

Confocal microscopy has become a vital technique for life sciences due to higher lateral and axial resolution it provides compared to standard epifluorescence microscopy. Improved axial resolution increases sectioning capabilities of the microscope, allowing for the observation of living specimens in three dimensions using image reconstruction.

Despite these, accessibility to confocal microscopes did not escalate in proportion to its usage around the globe. Therefore, in this thesis, we present a home-built laser scanning confocal microscope (LSCM) setup using commercially available equipment. The design of the setup was realized using a 488 nm laser beam, an inverted microscope, a photon multiplier tube (PMT) and optical/opto-mechanical parts including mirrors, lenses, beamsplitter, scan lens. In addition, X-Y axis galvanometer scanner was employed for beam steering. Instrumentation was made using a DAQ card and LabVIEW based software. For characterization purposes, confocal images of calibration samples were obtained.

As an alternative approach to standard LSCM, digital micromirror device (DMD) chip was implemented to confocal configuration for scanning the laser beam on specimen. Being cost-efficient and digital makes DMD-based scanners a promising candidate to be used in optical microscopy. Two different scanning algorithms were developed to modulate array of mirrors on DMD chip and results were compared accordingly.

## ÖZETÇE

Konfokal mikroskopi standart yansıma floresans mikroskopiye kıyasla sağladığı daha iyi yanal ve eksenel çözünürlük nedeniyle son yıllarda önemli bir teknik haline gelmiştir. İyileştirilmiş eksenel çözünürlük mikroskopun kesitleme yeteneğini artırarak canlı örneklerin imge yeniden oluşturma tekniği ile 3 boyutlu şekilde sergilenmesine olanak sağlamıştır.

Bunlara karşın, dünyada artan kullanıma oranla konfokal mikroskopa erişim kolaylaşmamıştır. Bu nedenle, bu tezde, ticari olarak erişilebilir bileşenlerden oluşturulmuş, laboratuvar ortamında geliştirilmiş lazer taramalı konfokal mikroskop düzeneği sunulacaktır. Düzenek tasarımı 488 nm dalgaboyunda bir lazer ışını, ters mikroskop, foton çoklayıcı tüp ve ayna, mercek, ışınbölücü, tarama lensi gibi optik ve optomekanik parçalarla gerçekleştirilmiştir. Ek olarak, X-Y ekseninde tarama yapabilen galvanometrik tarayıcı aynalar ışın yönlendirme için kullanılmıştır. Enstrümantasyon geliştirilen LabVIEW temelli yazılım ve veri toplama kartı kullanılarak sağlanmıştır. Düzenegin performans testi için kalibrasyon örneklerinin konfokal görüntüleri alınmıştır.

Standart lazer taramalı konfokal mikroskopiye alternatif olarak, sayısal mikroayna aygıtı temelli optik tarayıcı konfokal düzeneğe eklenmiştir. Düşük maliyeti ve sayısal olması nedeniyle sayısal mikroayna aygıtı temelli tarayıcılar optik mikroskobide geleceği olan cihazlardır. İki adet farklı tarama algoritması aynaları sürmek için geliştirilmiş olup farklı yöntemlerle alınan imgeler buna göre karşılaştırılmıştır.

## ACKNOWLEDGMENTS

Two years at Koç University was an invaluable journey. I would like to start expressing my graditudes to Prof. Dr. Alper Kiraz, for providing me the opportunity to work in his laboratory and all the effort he has put in for me during my master. It has been an enlightening experience.

Secondly, i thank to Adnan Kurt for giving me the insight whenever i was faced with a problem to solve during my studies. His mentorship has been very meaningful for me and i will always remember how helpful he was.

I also thank to Selçuk Çakmak for his help in hardware/software development of both setups at any time i needed.

Last but not least i would like to thank to Gamze Gül for her infinite supply of lecture notes.

## TABLE OF CONTENTS

<b>List of Figures</b>	<b>vii-x</b>
<b>Chapter 1: Introduction</b>	<b>1</b>
1.1 Optical Microscopy Fundamentals	1-8
1.2 Confocal Microscopy	9-13
1.3 Digital Micromirror Device	13-14
<b>Chapter 2: Experimental Setup</b>	<b>15</b>
2.1 Galvanometric Optical Scanner Based Confocal Microscope Setup	15-22
2.2 Confocal Microscope Setup Utilizing DMD-Based Optical Scanner	22-25
<b>Chapter 3: Results and Discussion</b>	<b>25</b>
3.1 Instrumentation of Galvanometric Optical Scanner Based Confocal Microscope and Obtained Results	25-36
3.2 Results Obtained with DMD-Based Optical Scanner	36-43
<b>Chapter 4: Conclusion</b>	<b>43</b>
<b>References</b>	<b>44</b>

## LIST OF FIGURES

Figure 1.1: Single Lens Magnification Illustration.....	1
Figure 1.2: Compound Microscopy.....	2
Figure 1.3: Critical Illumination Illustration.....	2
Figure 1.4: Transmitted and Reflected Images of Bubbles in Film.....	3
Figure 1.5: Illustration of Darkfield and Brightfield Microscopy.....	3
Figure 1.6: Köhler Illumination.....	3
Figure 1.7: Numerical Aperture in Microscopy.....	4
Figure 1.8: Representation of Rayleigh Criterion.....	4
Figure 1.9: Relationship Between Index of Refraction Light Acceptance.....	5
Figure 1.10: Finite and Infinity Optical Systems.....	5
Figure 1.11: Epifluorescence Microscopy.....	6
Figure 1.12: Illustration of STED Setup and Comparison of Obtained Results with STED Microscopy to Confocal Microscopy.....	7
Figure 1.13: Confocal Microscope Patent Drawing.....	7
Figure 1.14: Confocal and Widefield Imaging Comparison.....	8
Figure 1.15: Laser Scanning Confocal Microscopy.....	9
Figure 1.16: Nipkow Disk Configuration.....	9
Figure 1.17: Illustration of PMT Working Principle.....	10
Figure 1.18: Lateral and Axial Resolutions in Widefield and Confocal Microscopy.....	10
Figure 1.19: 3D Reconstruction of Sunflower Pollen Grain by Sectioning.....	11
Figure 1.20: DMD Illustration.....	11
Figure 1.21: DLP3000 dimensions.....	12



Figure 2.1: Illustration of Opto-Digital Confocal Microscope Setup.....	12
Figure 2.2: Photograph of the Opto-Digital Confocal Microscope Setup.....	13
Figure 2.3: Photograph of the Laser Source.....	13
Figure 2.4: Galvanometer Scanner Mirrors with Incoming and Reflected Beam Path.....	14
Figure 2.5: Illustration of Scan Lens Working Principles.....	14
Figure 2.6: Photograph of the Inverted Microscope Body.....	15
Figure 2.7: Stock Images of Used Objectives.....	16
Figure 2.8: Photograph of Widefield Imaging System.....	16
Figure 2.9: The Beamsplitter and Point Detection System.....	17
Figure 2.10: BNC Connections to DAQ Connector.....	18
Figure 2.11: Photograph of LightCrafter and Illustration of Its Hardware.....	19
Figure 2.12: Interface of the LightCrafter Software.....	19
Figure 2.13: Photograph of the DMD-based Imaging Setup.....	20
Figure 3.1: Working and Integration Progress of Potential Supply.....	21
Figure 3.2: Interface of the initial version of A2K2.....	21
Figure 3.3: Raster Scan Illustration.....	22
Figure 3.4: Block Diagram of the Initial Version of A2K2.....	22
Figure 3.5: Block Diagram of “Init.vi” .....	23
Figure 3.6: Block Diagram of “Scan.vi” .....	24
Figure 3.7: “Params” Cluster.....	24
Figure 3.8: “VoltageFactors” Cluster.....	25
Figure 3.9: Waveform Graph of the Applied Potential to the Scanner Mirrors.....	25
Figure 3.10: Block Diagram of the “Close.vi”.....	26
Figure 3.11: Scan Parameters of Revised Version of Software.....	26

Figure 3.12: Developer Scan Parameters and Widefield Imaging.....	27
Figure 3.13: Block Diagram of Bidirectional Algorithm and Produced Waveform.....	27-28
Figure 3.14: Image of Microruler with Ghosting Distortion, 100x100 pixel number.....	28
Figure 3.15: Interface of the Improved Software.....	29
Figure 3.16: Block Diagram of A2K2 v1.5.....	29
Figure 3.17: Confocal Images of Microruler and Cd-Pattern, 1000 x 1000 pixel number.....	30
Figure 3.18: Oscilloscope Data of LightCrafter Operating in Image Sequence Mode with 1 Hz frequency.....	30
Figure 3.19: Produced Images of Single Spot Scanning Algorithm.....	31
Figure 3.20: Example Image of a Multi Spot Scanning Algorithm.....	31
Figure 3.21: Comparison of images with diffuser being stationary and moving (40x 0.55NA)...	32
Figure 3.22: Comparison of images with diffuser being stationary and moving (60x 1.49NA)...	32
Figure 3.23: Single Spot Scanning of Microruler, 4.4 kHz Scanning Frequency.....	33
Figure 3.24: Diffuser Moving 4 kHz Scan Speed, All Mirror Off, Single Spot Scanning and Multi Spot Scanning Results.....	33
Figure 3.25: Current Source Follower Circuit.....	34
Figure 3.26: Interface and Block Diagram of Camera Triggering Program.....	35
Figure 3.27: Post-processed Image Result with Range Filter on Left Hand Side and Standard Filter Result on Right Hand Side.....	36
Figure 3.28: Image Obtained with All Mirrors in Off Position and Intensity Profile along the Chosen Line. (Mean = 239.62, Standard Deviation = 19.87, Signal to Noise Ratio = 12.05).....	36
Figure 3.29: Image Obtained with Single Spot Scanning and Intensity Profile along the Chosen Line. (Mean = 35.27, Standard Deviation = 7.16, Signal to Noise Ratio = 4.92).....	37
Figure 3.30: Image Obtained with Multi Spot Scanning and Intensity Profile along the Chosen Line. (Mean = 21.56, Standard Deviation = 4.03, Signal to Noise Ratio = 5.34).....	37
Figure 3.31: Image Obtained with Multi Spot Scanning and Intensity Profile along the Chosen Line. (Mean = 20.01, Standard Deviation = 6.12, Signal to Noise Ratio = 3.26).....	38

## Chapter 1: Introduction

### 1.1 Optical Microscopy Fundamentals

Mankind's involvement with optics goes back to ancient times[1], with first primitive lenses being invented around 700 - 750 BC. It generated significant attraction among scientists and philosophers of early civilizations as people were keen on understanding what things were made of. Starting with the invention of magnifying objects, over the course of the years humans have developed theory of optics and found many uses in daily life with ever improving new imaging techniques and methods. For a single thin lens, magnification is given by[2]

$$M = \frac{f}{f - d_i}$$

where  $f$  is the effective focal length and  $d_i$  is the distance from object to lens. After its invention, single imaging lenses were used for magnification or sunlight collimating purposes.

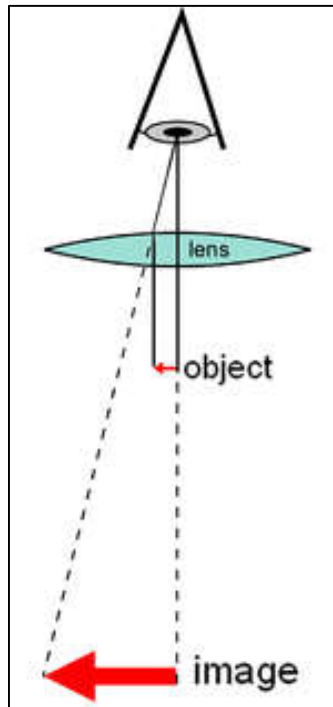


**Figure 1.1 Single Lens Magnification Illustration[2]**

At early 1600s in Europe, people have designed and produced more complex imaging systems known as “compound microscopes” which included usage of more than a single lens for magnification[3]. Consisting of two converging lenses, first lens focuses the light reflected from an object into an intermediate plane between two lenses where the second lens (also called as an eyepiece) collimates the light and sends the formed magnified image to human eye[4]. For such design, magnification is equal to ratio of effective focal length of eyepiece to effective focal length of object lens. These setups are defined as classical microscopes and called finite optical system. One of the most famous researcher of the era was Robert Hooke, where he has studied biological samples utilizing compound microscopy principles with the microscope built by himself[5].

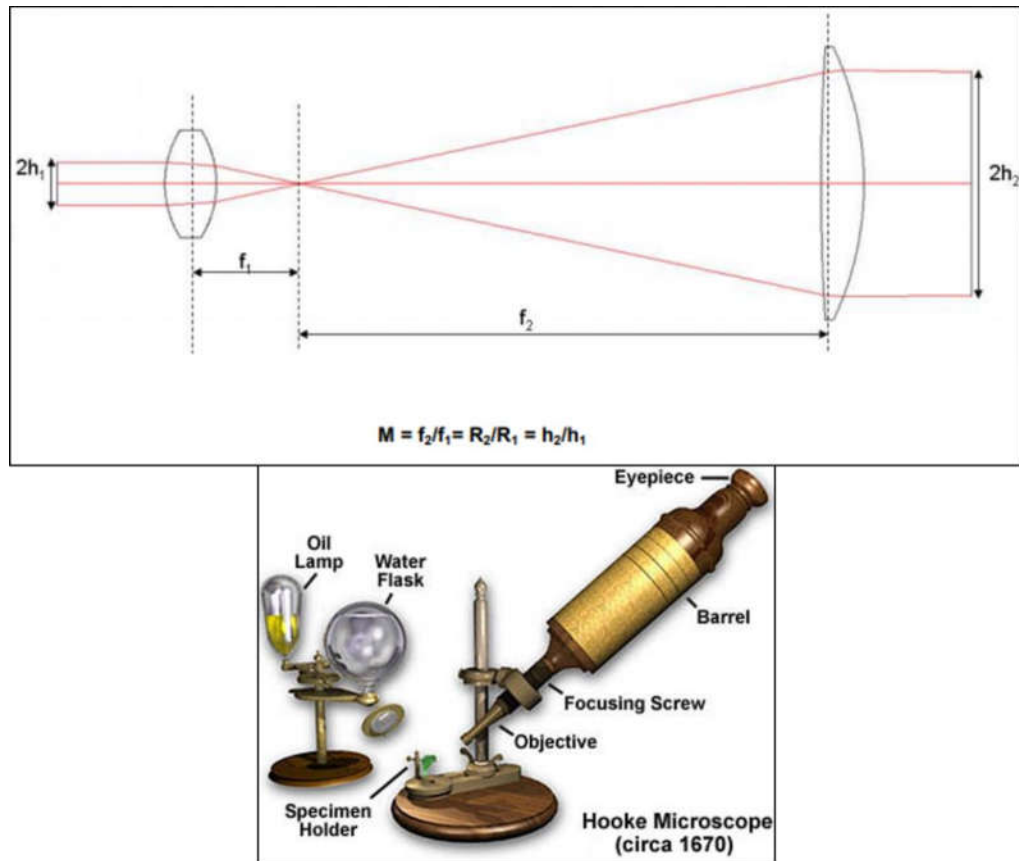


**Figure 1.2 Compound Microscopy[4,5]**

One important aspect in optical microscopy is the sample illumination as it drastically affects the obtained image quality and defines a classification of microscopy techniques. Classical sample illumination contains a light source with a condenser lens, described as critical illumination[6].

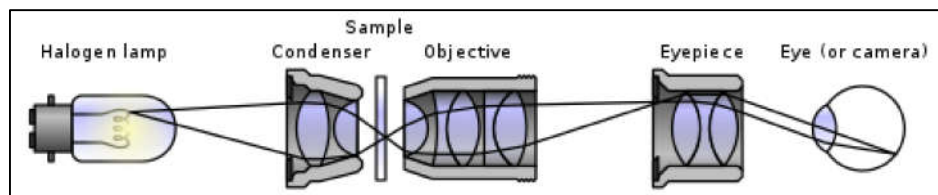


**Figure 1.3 Critical Illumination Illustration[6]**

If the illumination was made from back side of the sample, it has been defined as transmitted illumination. On the other hand, if the illumination was incident on front side of the sample and reflected beams are being collected, it has been defined as reflected(epi) illumination[7].



**Figure 1.4 Transmitted and Reflected Images of Bubbles in Film[7]**

Both illumination types consists of two different methods, when the sample is illuminated with a perpendicular incident light it has been described as brightfield illumination[8]. On the other hand, if the light coming from the source is blocked in a setting that only rays at an oblique incidence angle reaches the sample, the method is described as darkfield illumination[8]. It provides sharper contrast in the sample image, however the trade-off is the image may lack desired light levels.

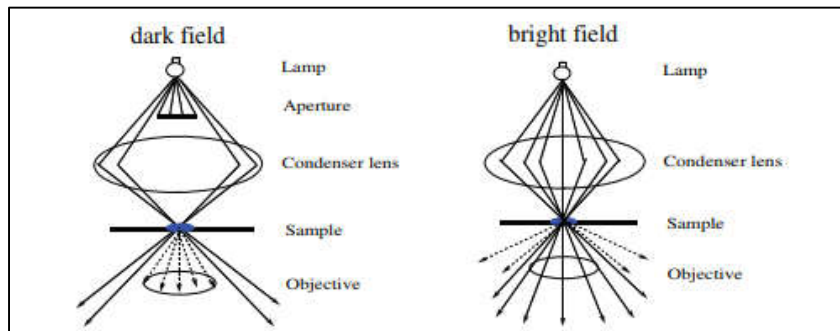


**Figure 1.5 Illustration of Darkfield and Brightfield Microscopy[9]**

In modern microscopy, illumination standard is defined by double diaphragm or more famously known by its inventor's name, Köhler illumination[8]. Köhler illumination technique ensures uniform illumination of the specimen and prevents ghosting and flares in the image plane. In addition to a light source and condenser, two additional lenses namely collector lens and relay(field) lens is present and it utilizes two diaphragms where the one placed in front of the collimating lens of the light source, called as field diaphragm. Broadness of the field diaphragm allows to determine amount of light used in illumination, which is critical for adjustments of contrast level and resolving power dependent on specimen. The second diaphragm, aperture diaphragm, enables controlling the properties of conjugate image of filament. This corresponds to tuning of brightness in field of view[10].

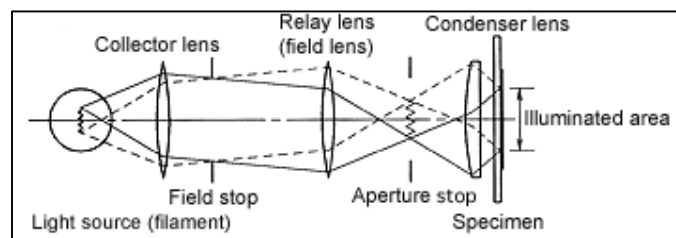


**Figure 1.6 Köhler Illumination[10]**

Another important optical phenomenon in optical microscopy is numerical aperture, which is directly related to precision of a microscope's to capability of solving tiny details in sample or simply, resolution. Numerical aperture is a property of a microscope objective defining how much light can enter the objective. With formulation given below[11]

$$NA = n * \sin \alpha$$

where  $n$  is the index of refraction of the medium and  $\alpha$  is the half of the maximum angle of rays from a point source entering the objective.

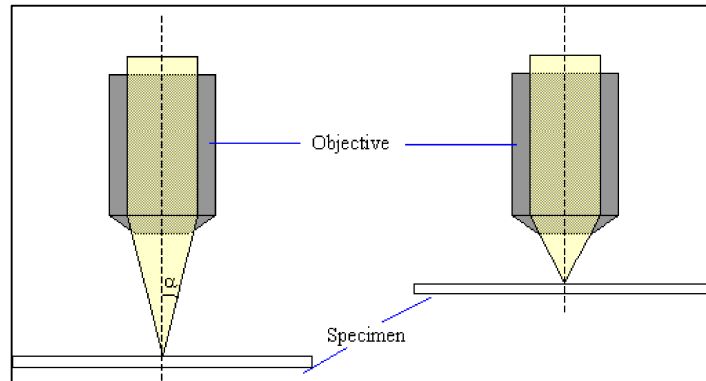


**Figure 1.7 Numerical Aperture in Microscopy[11]**

Resolution in optical microscopy has the definition of smallest distance that can be resolved between two points on a sample[12]. The nature of resolution in optical microscopy can be understood by looking at properties of light. In microscopy, as the rays of an incoming beam is focused on a spot in image plane of an objective, it will be diffracted. This diffraction has a form that can be described by airy functions, therefore the name airy disks will be formed in image plane. If the disks overlap, then the spot on the sample cannot be distinguished and blurring will appear on image. The minimal separation distance in image plane to be resolved is defined by Rayleigh Criterion. Rayleigh Criterion is described as minimal resolvable separation between two points of equal intensity which corresponds to overlapping of one point's maximum intensity in first airy disk to second point's minimum intensity in its first airy disk.

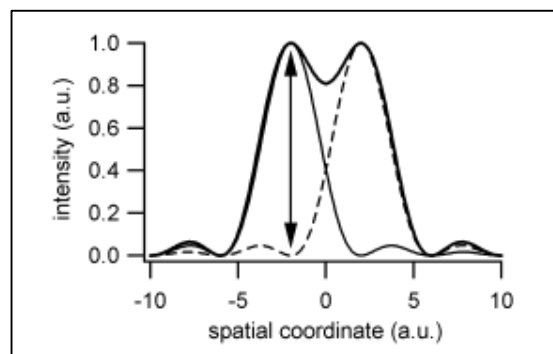


**Figure 1.8 Representation of Rayleigh Criterion[12]**

Rayleigh criterion is therefore given by the equation[12]:

$$r = \frac{0.61 * \lambda}{NA}$$

where  $\lambda$  is the wavelength of the light source. Therefore, resolution in optical microscopy has its limitations due to diffractive nature of light. To increase lateral resolution, light sources with wavelength in ultraviolet region are sometimes preferred. In addition, microscope objectives that operate in oil or water medium has been developed due to index of refraction of pure water being  $n=1.33$  and immersion oil being  $n=1.51$ [13]

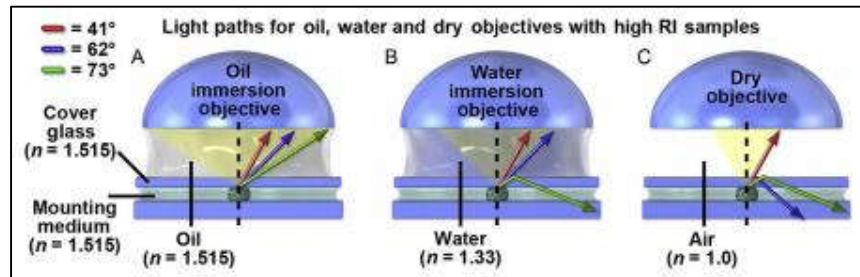


**Figure 1.9 Relationship Between Index of Refraction and Light Acceptance[13]**

In order to increase the capabilities of optical microscopy, several design rules have been standardized in modern day microscopy. One of them is usage of infinity corrected systems. As shown in figure 1.2, early microscopes had an exact length with components being secured in a finite length tube, since rays were focused in an intermediate plane between objective and eyepiece. However, modern microscopy has adopted infinity corrected systems, where a special lens named tube lens being used in between eyepiece and objective[14].

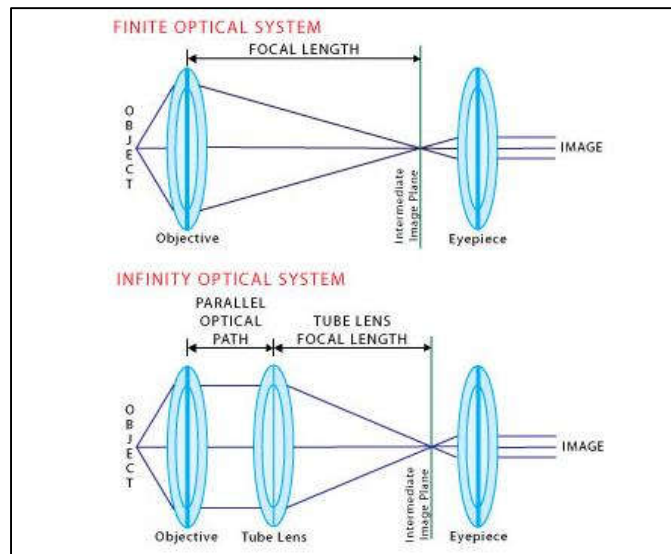


**Figure 1.10 Finite and Infinity Optical Systems[14]**

Advantage of infinity corrected system design stems from flexibility of selection of separation distance between objective and tube lens. This allows additional optical components such as beamsplitters, filters, dichroic mirrors to be implemented to system for enhancing capabilities of microscopes without aberrations. One of the microscopy techniques that utilizes and builds upon infinity corrected system is epifluorescence microscopy, where sample is illuminated with a specific wavelength of light resulting in excitation and fluorescence[15]. Fluorescent beam then follows the same path and filtered with a dichroic mirror, which is sent to a camera or eyepiece.

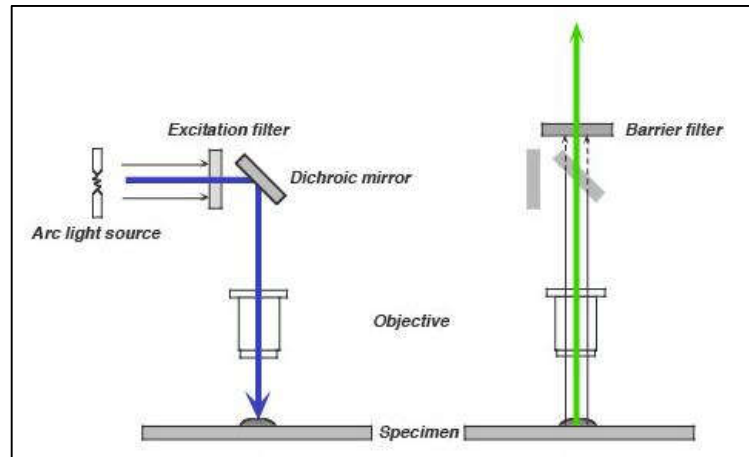


**Figure 1.11 Epifluorescence Microscopy[15]**

Another definition of resolution in microscopy was made by Ernst Karl Abbe in 1873[16]:

$$d = \frac{\lambda}{2 * NA}$$

Improvements and emerging of different techniques in optical microscopy have reached to an unprecedented level in recent years. One of the most important advancements in the area was the invention of Stimulated Emission Depletion (STED) microscopy technique[17,18] awarded a nobel prize in 2014 in chemistry by breaking the Abbe's resolution limit and achieving less than 30 nm, therefore pioneering the field nanoscopy. Two lasers are employed in STED microscopy, one being the excitation laser for fluorescence microscopy. The second laser, also known as STED laser, has a shape of donut and wavelength of excitation of the specimen. Therefore, only a small portion of fluorescence is imaged by the detector.



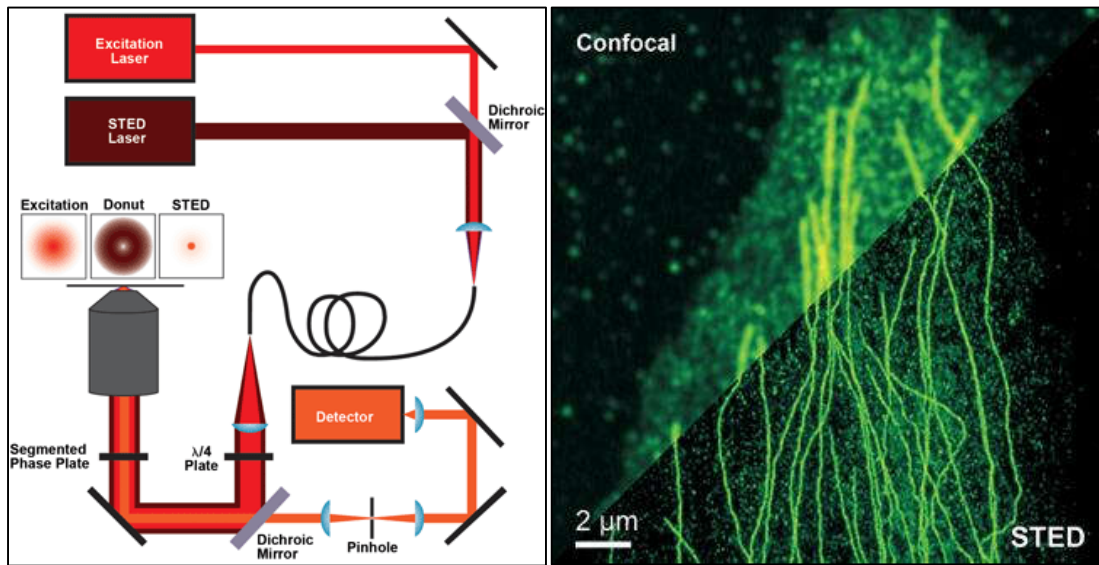


**Figure 1.12 Illustration of STED Setup and Comparison of Obtained Results with STED Microscopy to Confocal Microscopy[17]**

Another technique that has gained more attraction in recent years particularly in life sciences is laser scanning confocal microscopy, which is explained in next section.

## 1.2 Confocal Microscopy

Confocal microscopy was first patented by whom famously known for works in Artificial Intelligence, Marvin Minsky in 1957, as an improvement upon standard epifluorescence microscopy[19]. The word “confocal” means sharing the same focal distance[20].

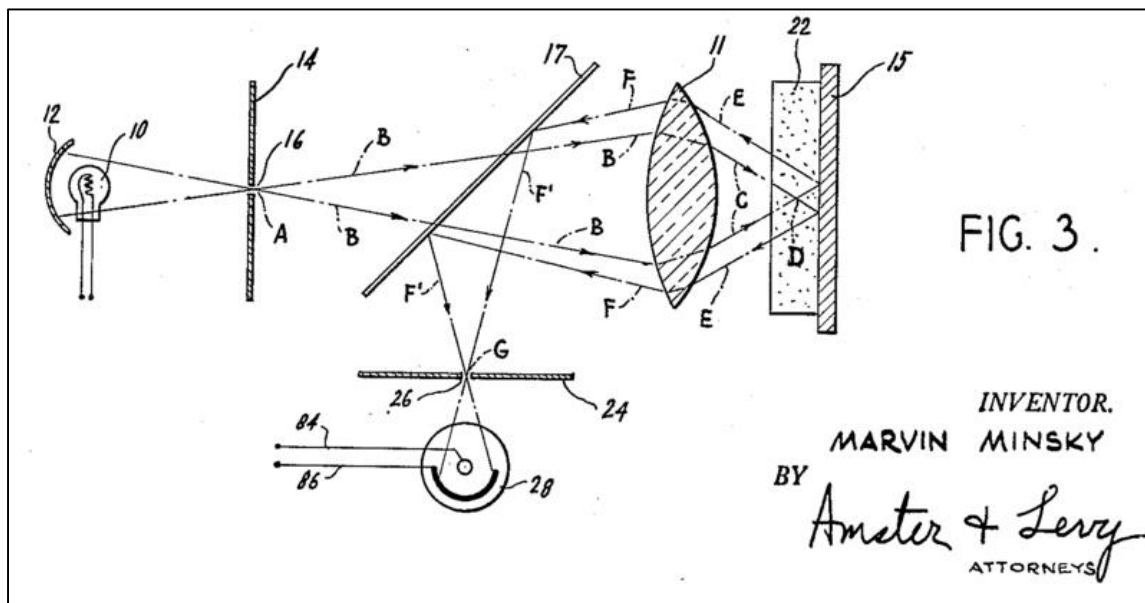


**Figure 1.13 Confocal Microscope Patent Drawing[19]**

However, it took about thirty years for the first commercial confocal microscope to emerge. In modern microscopy, a “confocal microscope” corresponds to a point by point illumination of a specimen by a laser beam and using a point detector with a pinhole in front of it respectively. The point by point illumination reduces the background noise in the reflected beam. In addition, the pinhole in front of the point detector blocks the stray light further increasing the spatial resolution.

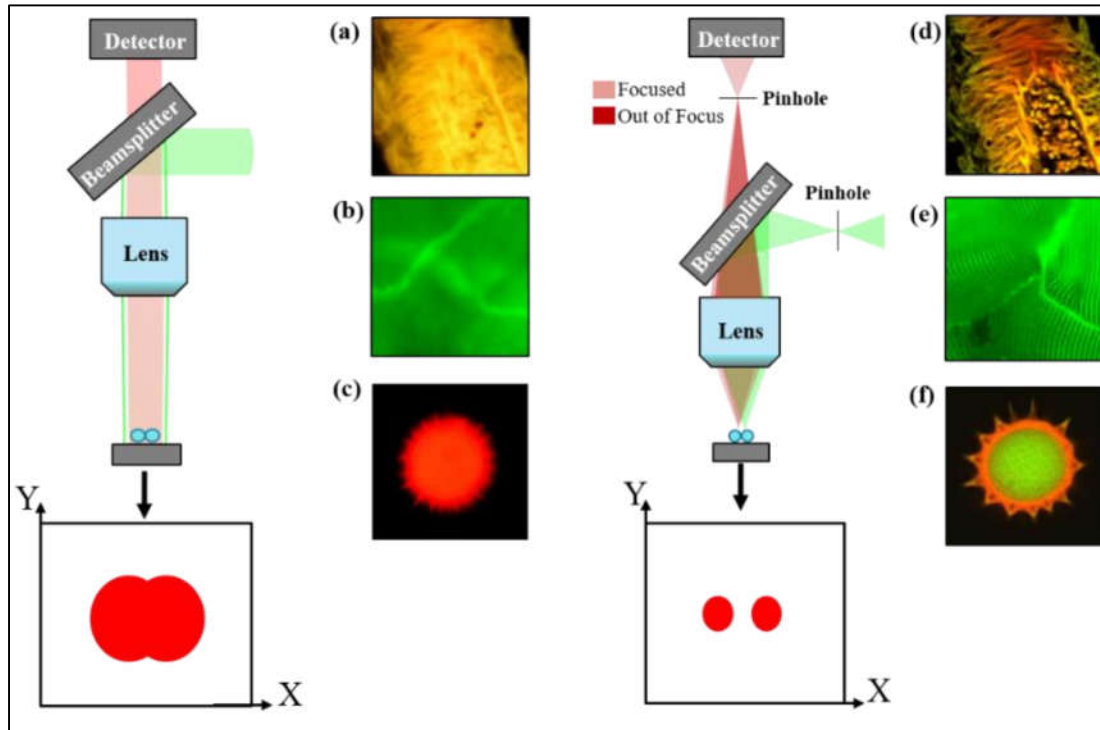


**Figure 1.14 Confocal and Widefield Imaging Comparison[21] a) Widefield Image of Medulla b) Widefield Image of Rabbit Muscle Fiber c) Widefield Image of Sunflower Pollen Grain d) Confocal Image of Medulla e) Confocal Image of Rabbit Muscle Fiber f) Confocal Image of Sunflower Pollen Grain**

There are three main configurations in confocal microscopy for realizing point by point scanning. Point by point scanning can be carried out by moving sample plate of specimen however, this method has been abandoned over steering light by using galvanometer scanning mirrors due to limitations of speed. In a standard galvanometer scanner, system is driven by an analog signal, where one of the mirrors directs the light for moving in x axis whereas the second mirror projects the light for movement in y axis in image plane by rotation of mirrors. Using a raster scan algorithm, scanning is carried out on the specimen.

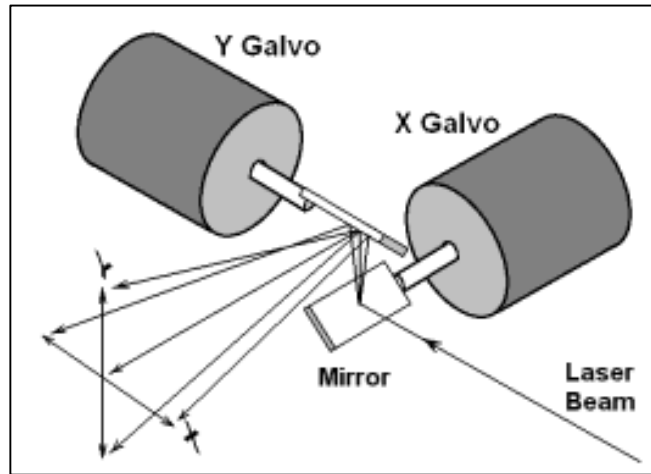


**Figure 1.15 Laser Scanning Confocal Microscopy[22]**

The downside of the standard laser scanning confocal microscopy is dependent on scanning area and sampling rate, it can be slow. To decrease the time required for image acquisition, multiple point illumination on the sample has been utilized using Nipkow disk configuration. The trade-off is that such configuration is expensive compared to standard laser scanning confocal microscopy.

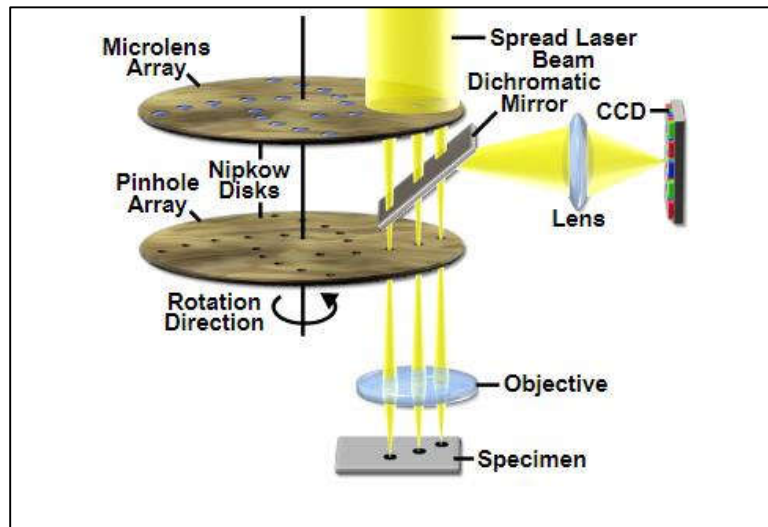


**Figure 1.16 Nipkow Disk Configuration[23]**

As detector, multiple options are available such as photomultiplier tube (PMT), charged coupled device (CCD) cameras or photodetector[24]. The most common used detector, PMT, is a device that uses the photoelectric effect. An incoming beam shines upon a photocathode causing electrons to be excited and detached from the surface. Then, excited electrons are accelerated and sent towards dynodes where they get multiplied to be finally collected by an anode. The created current is then converted to an electric signal to be processed.

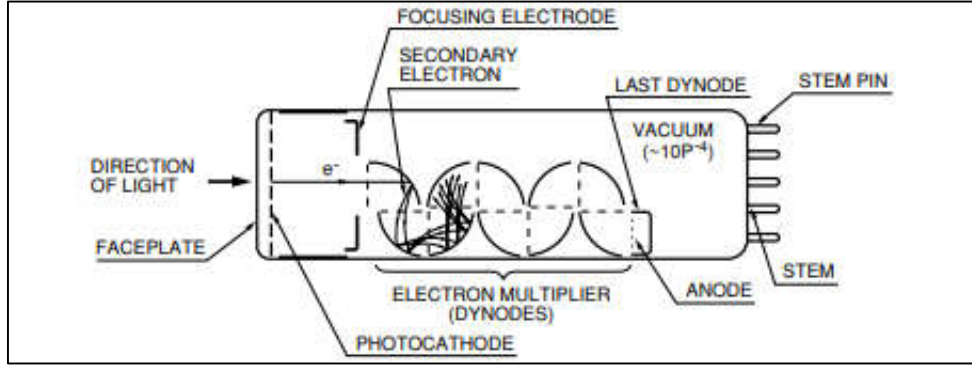


**Figure 1.17 Illustration of PMT Working Principle[25]**

To better understand the power of confocal configuration and effect of pinhole in front of the detector, one must again turn to theory of optics. As mentioned earlier, the focused light on image plane will diffract as imaging system's response, this function is called Point Spread Function (PSF) and the first order of diffraction is nothing, but Airy Disk as explained in section 1.1[12]. In confocal microscopy design, response function of the imaging system corresponds to square of PSF[12]. Point spread function of an optical microscope is given by

$$PSF(\rho, \varepsilon) = \left( \frac{\sin(\frac{\varepsilon}{4})}{\frac{\varepsilon}{4}} \right)^2 * \frac{2J_1^2(\rho)}{\rho^2}$$

With  $J_1$  being first order bessel function of  $\rho$ ,  $\rho$  being a function of lateral coordinates  $r$  and  $\varepsilon$  being a function of axial coordinates  $z$  given as

$$\rho(r) = \frac{2\pi}{\lambda} * r * NA \quad \varepsilon(z) = \frac{2\pi}{\lambda} * NA^2 * z$$

respectively. Computed results for 488 nm wavelength and 0.55 NA are presented in figure 1.18.

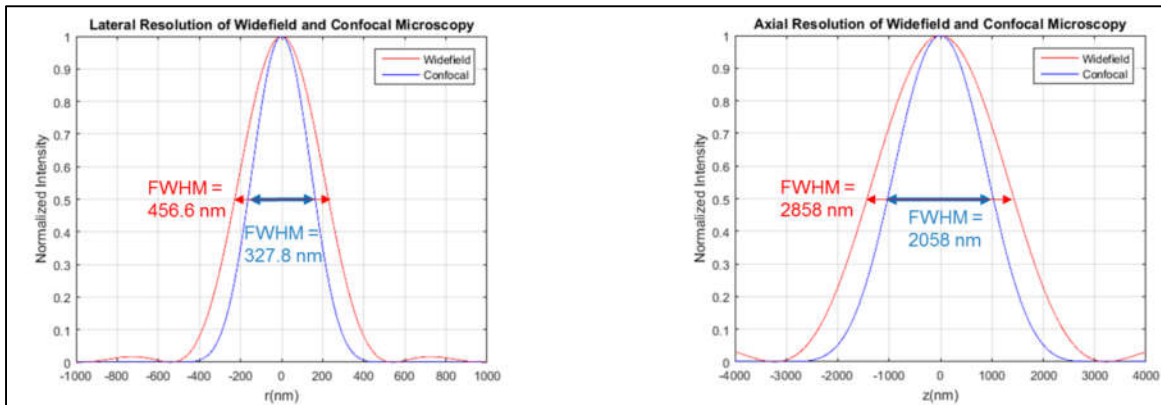


**Figure 1.18 Lateral and Axial Resolutions in Widefield and Confocal Microscopy**

As it can be seen from figure x both the lateral and axial resolutions are improved in confocal microscopy. In addition, second and higher order diffractions of point spread function are not present in confocal configuration which explains the reduced background noise in a qualitative manner. Axial resolution improvement and reduced background noise allows images at different sections in the specimen to be resolved. Sectioning capability is the point where confocal microscope really shines, as using image processing techniques, images taken at different sections can be reconstructed[21]. This feature of confocal microscopy allows the 3D demonstration of living cells which has become crucial for life sciences in recent years.

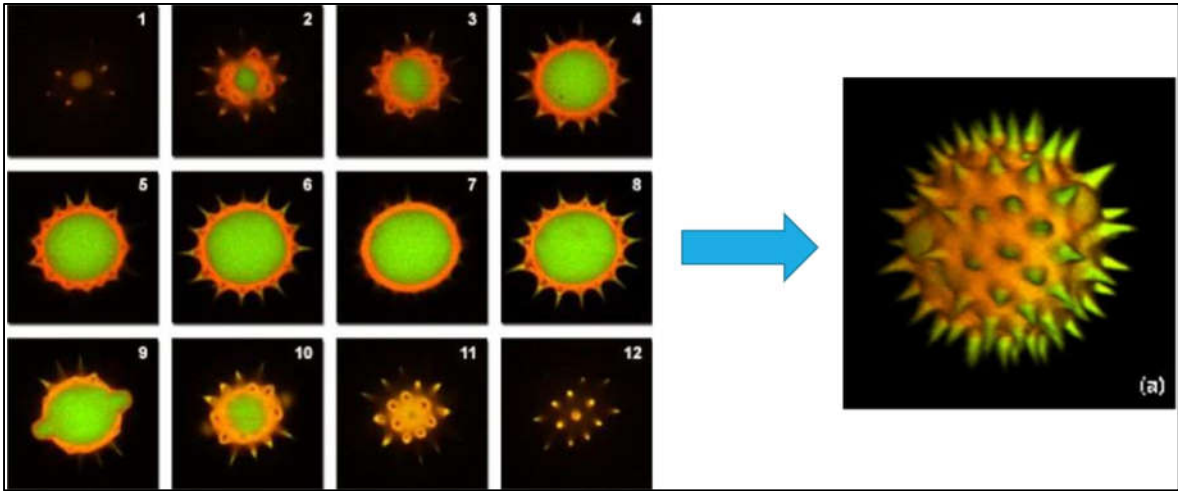


**Figure 1.19 3D Reconstruction of Sunflower Pollen Grain by Sectioning[21]**

### 1.3 Digital Micromirror Device

Digital micromirror device is a chip developed by Texas Instruments, which is in family of microelectro-mechanical (MEMS) devices. In its core, a DMD consists of an array of micron sized mirrors that can modulate light by being in either “on” or “off” state. The chip that has been used in our studies, DLP3000, consists of 608 x 684 mirrors which can either be in two positions as mentioned, +12 degree or -12 degree[26,27].

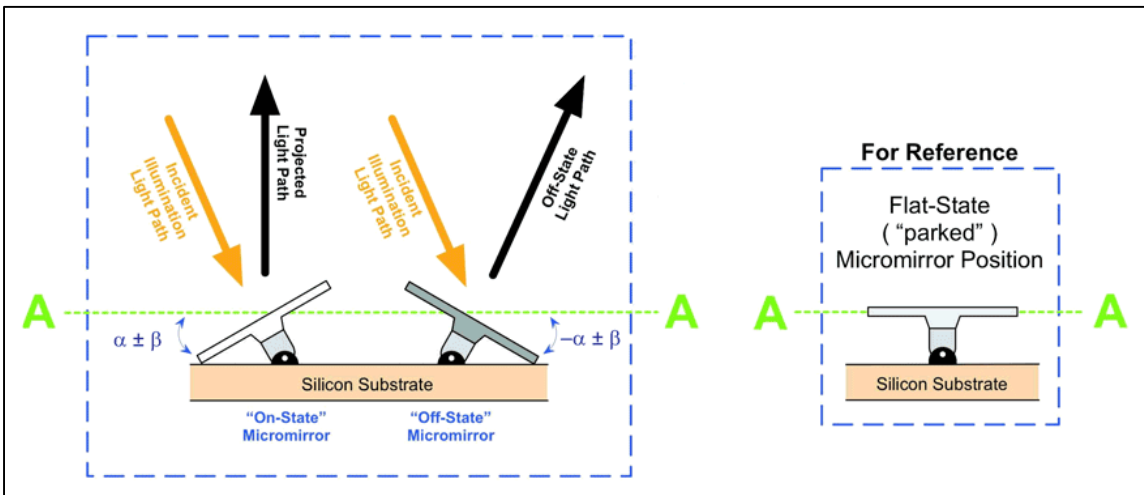


**Figure 1.20 DMD Illustration[27]**

DMD chips find themselves many uses such as usages in projection, maskless lithography, mounted displays, phase modulators[28,29,30,31]. Being relatively cheap, digital and fast are the properties that makes these chips promising for many applications. One of the active research topics is their usage in optical microscopy[32, 33, 34, 35]. Our interest of DMD was in beam steering as a replacement for galvanometer scanner mirrors and to test whether it could produce image quality like one obtained with conventional confocal microscopy.

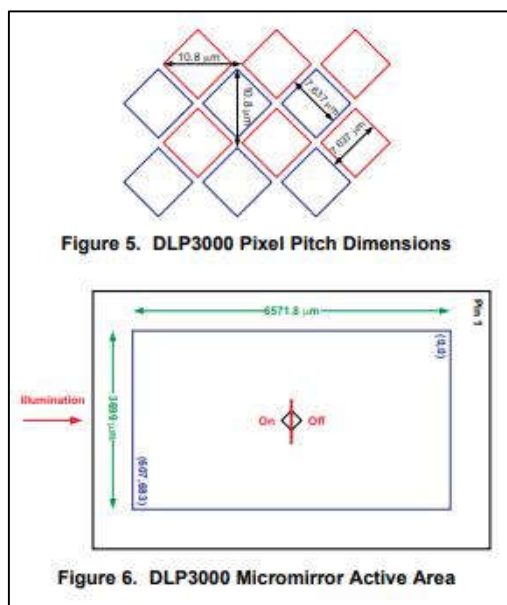


Figure 1.21 DLP3000 Dimensions

## Chapter 2: Experimental Setup

### 2.1 Galvanometric Optical Scanner Based Confocal Microscope Setup

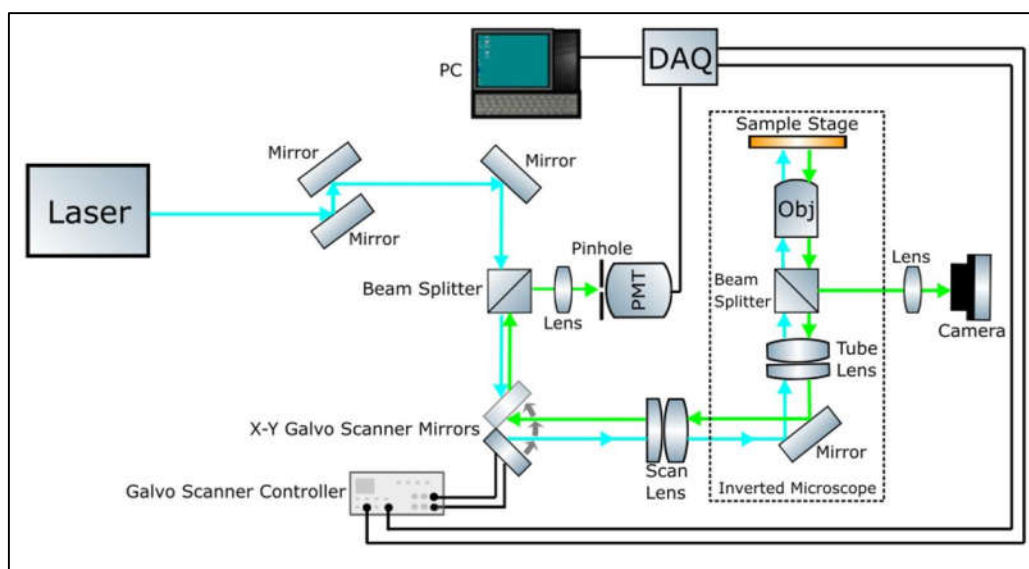
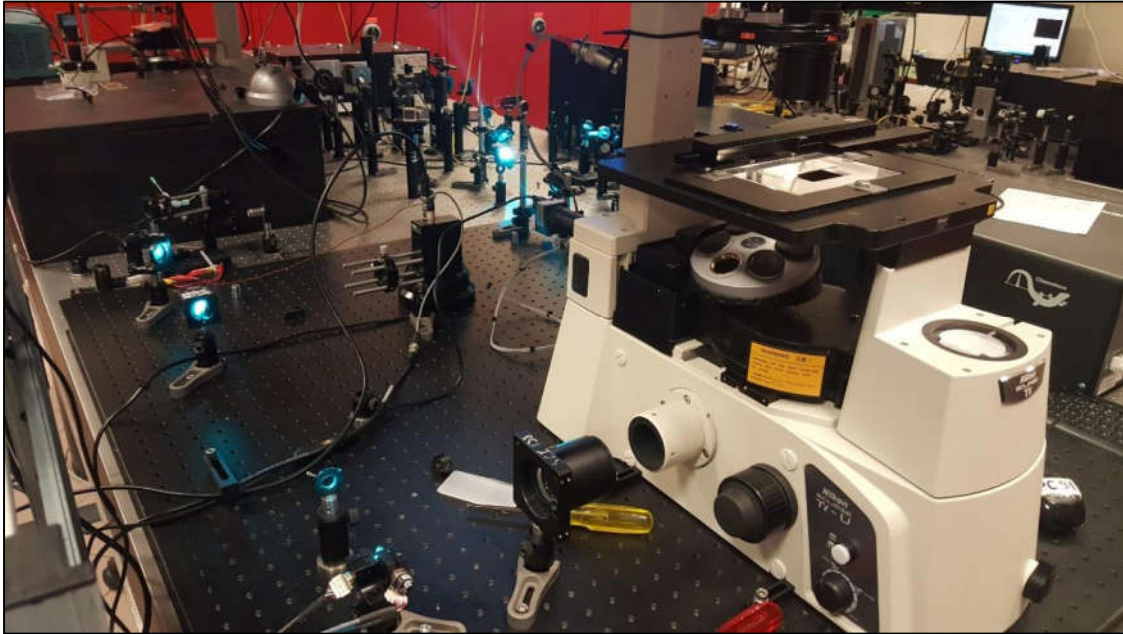


Figure 2.1 Illustration of Opto-Digital Confocal Microscope Setup



In this work we have built a custom confocal microscopy setup in lab environment. It consists of a laser light source, mirrors, beamsplitter, galvanometer scanner mirrors, scan lens, inverted microscope, objective, CMOS camera, achromat lens, PMT and data acquisition(DAQ) card.



**Figure 2.2 Photograph of the Opto-Digital Confocal Microscope Setup**

The laser light source was a laser from Coherent with a frequency doubler in front of it, where it was possible to work with any wavelength of selection in the visible spectrum. Studies were performed using laser light with 488 nm wavelength and 5 mW power. After reflected from a periscope and a mirror for alignment purposes, light was directed to galvanometer scanner mirrors.



**Figure 2.3 Photograph of the Laser Source**

For light steering purposes two axis galvanometer scanner from Cambridge(6210H) was used. One of the mirrors directs light for scanning in x axis and the other mirror rotates for scanning in y axis scan thus, completing a raster scan on specimen. The mirrors have  $100\ \mu\text{s}$  small angle step size and 40 degrees mechanical rotation freedom[36]. With mirror sizes of 22.3 mm to 9.5 mm, scanners are relatively small and fast, applicable for applications with beam diameters from 3 to 7 mm which is suitable for confocal microscopy.

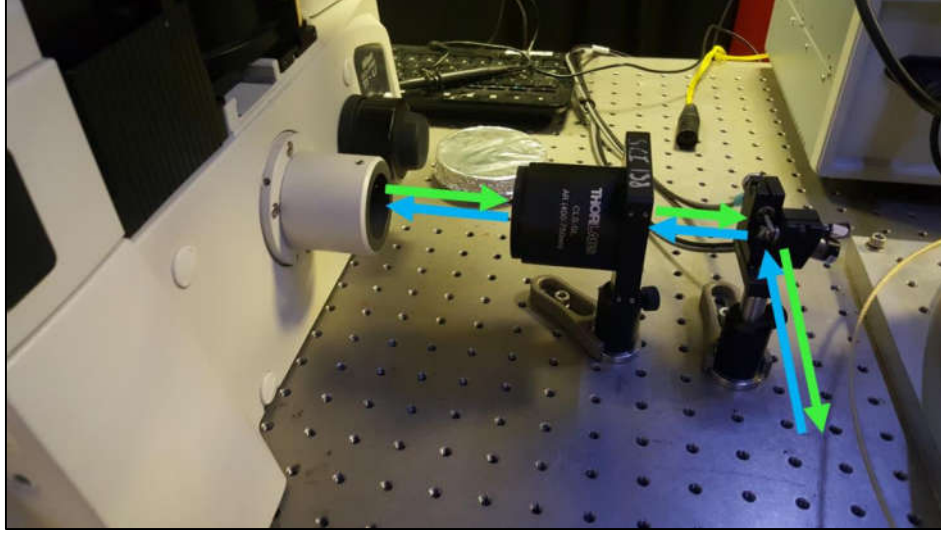


**Figure 2.4 Galvanometer Scanner Mirrors with Incoming and Reflected Beam Path**

As the incoming laser beam is reflected from galvanometer scanners, it is directed towards a special lens namely, scan lens. The scan lens is an essential optical component for laser scanning applications to prevent aberrations originating from the nature of laser scanning that the beam of light being strayed from aligned optical axis. In other words, scan lens ensures that regardless of deviation from the aligned optical axis, all the beam is focused in the same intermediate image plane without aberrations. In our studies CLS-SL model scan lens from Thorlabs Inc. was used. It has a working distance of 54 mm with maximum acceptable beam diameter of 4 mm[37].

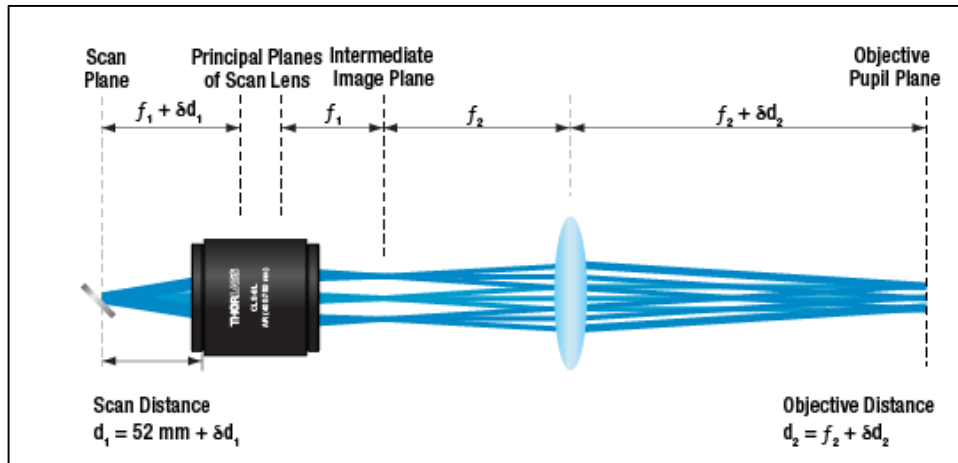


**Figure 2.5 Illustration of Scan Lens Working Principles[37]**



After the light passes through the scan lens, it goes inside to the inverted microscope, provided by Nikon with eclipse model Ti-U which has a mirror reflecting the beam upward to the tube lens with the focal length of 200 mm[38]. The reason behind the choice of name, “Opto-Digital” lies in the configuration of the inverted microscope. It has no binoculars so user working on the setup only interacts with it using a computer for image recording, after the placement of the sample and focusing of the laser beam was done. The microscope has a backport where a beamsplitter lying between the objective and tube lens directs the reflected beams towards this port. This feature allows the implementation of a camera for widefield imaging which can be of use for fast imaging of sample and helping to focus the incoming laser light.



**Figure 2.6 Photograph of the Inverted Microscope Body**

There were two objectives used in our studies one had a numerical aperture of 0.55 and 40x magnification whereas the oil immersion objective had 1.49 NA and 60x magnification[39].



**Figure 2.7 Stock Images of Used Objectives[39]**

Two calibration samples were used in the studies, one being a calibration ruler with strips having distance of  $10\ \mu\text{m}$  and a piece of CD-ROM for imaging its patterns. As mentioned above, reflected beam from samples were first directed to the backport of the microscope where it was sent to a CMOS camera namely DCC1240M with the achromatic doublet AC254-150-A-ML in front of it for imaging. Camera has the pixel number  $1280 \times 1024$ , monochrome sensor and a sensitive area of  $6.78 \times 5.43\ \text{mm}$ [40]. One important feature camera had was possibility of triggering the image capturing using an electrical signal which its role will become apparent in the chapter 3.

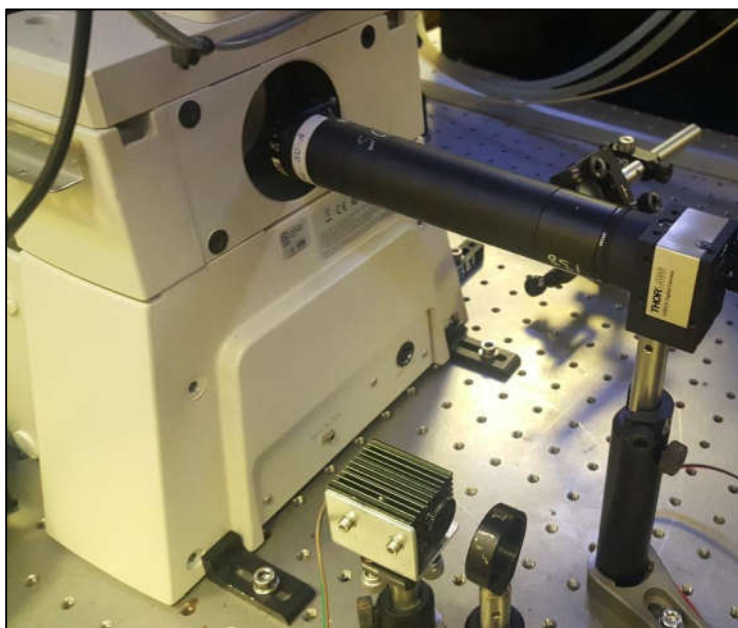


**Figure 2.8 Photograph of Widefield Imaging System**

As the beam follows the same path and gets de-scanned in scanner mirrors, it is separated with the usage of a beamsplitter provided by Thorlabs. After reflected from the beamsplitter, the beam is sent to the PMT with a focusing lens and pinhole of  $50\ \mu\text{m}$  diameter in front of it. The PMT(PMM02) from Thorlabs had a wavelength response between  $280\ \text{nm}$  and  $850\ \text{nm}$  and a control voltage between  $0$  and  $1.25\ \text{V}$  for adjusting its sensitivity[41]. As

the reflected beam finally reaches the PMT, point by point detection in the image plane was achieved.

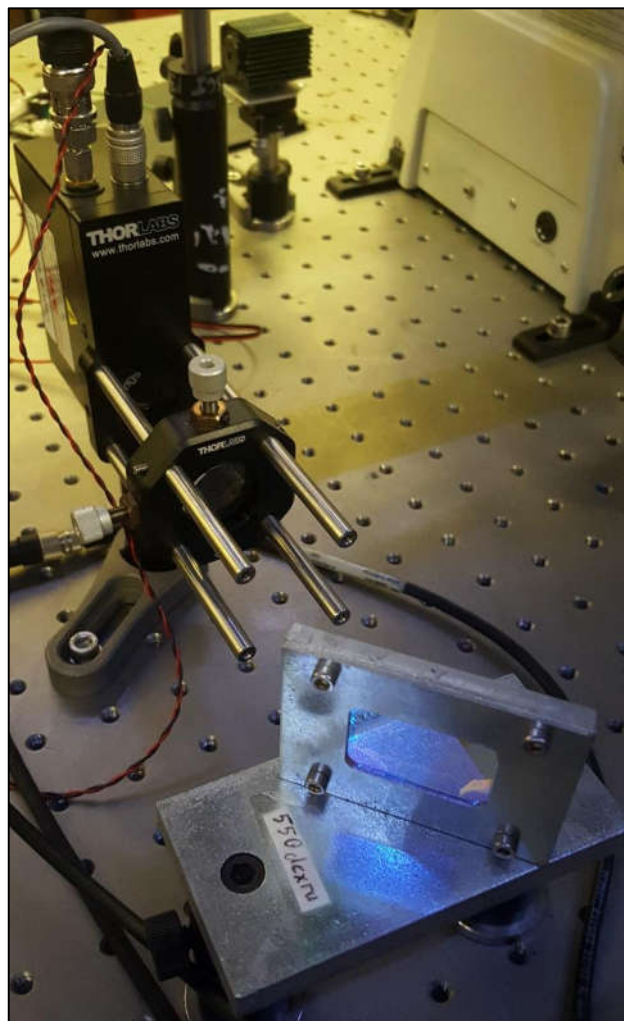


**Figure 2.9 Beamsplitter and Point Detection System**

The acquired signal from the PMT constitutes the confocal image and it is sent to NI DAQ card's analog input channel. In addition to storing and processing confocal data, the waveform signals for galvanometer scanner mirrors are generated using the DAQ card and sent from analog output channels to the mirrors. All this instrumentation was realized using LabVIEW based custom software developed in the laboratory, which is explained in detail in the proceeding chapter.

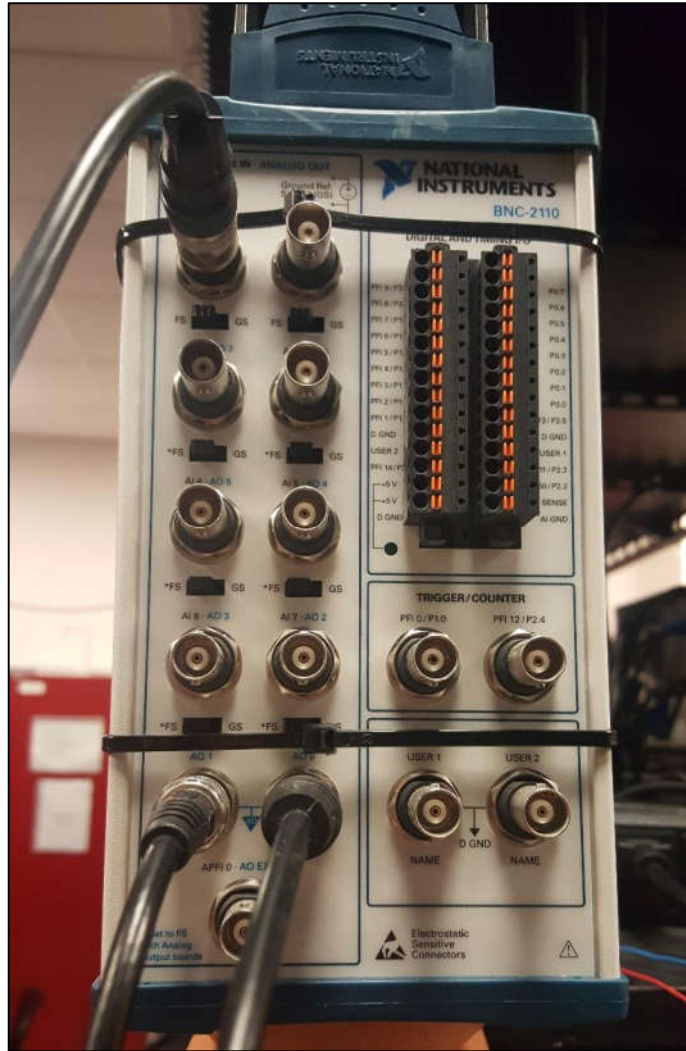


### Figure 2.10 BNC Connections to DAQ Connector

## 2.2 Confocal Microscope Setup Utilizing DMD-Based Optical Scanner

As mentioned earlier, to control the DMD chip DLP3000, the LightCrafter evaluation module from the Texas Instruments was used. Originally a pocket size projector, the LightCrafter comes with a control software and light engine, DMD controller board, processor-interface board hardware[42]. It features RGB light with 20L output, I/O trigger, 128MB NAND flash memory for image storage, 480p WVGA Resolution, FPGA programmability[42].

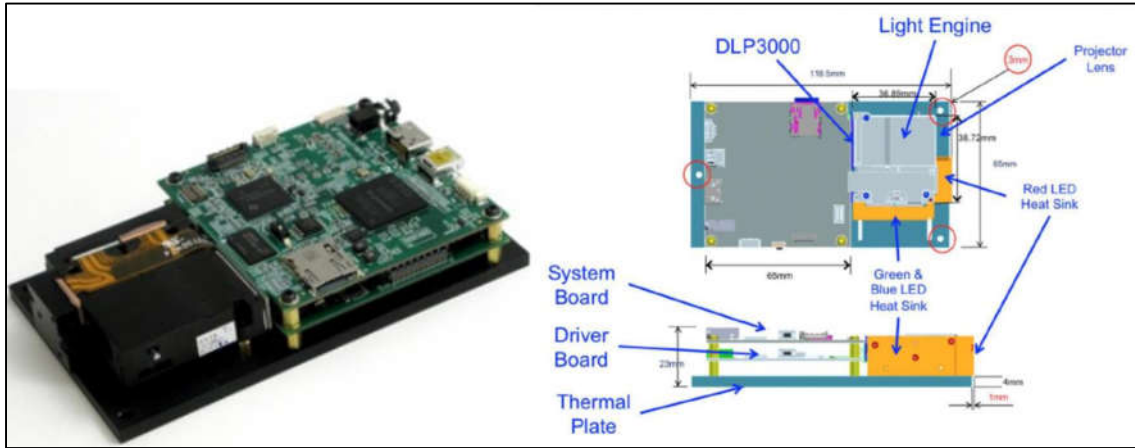


**Figure 2.11 Photograph of LightCrafter and Illustration of Its Hardware**

The built-in control software that comes with the LightCrafter operates in four different modes. The test pattern mode has coded patterns such as all mirrors off (solid black), all mirrors on (solid white), checkerboard which are useful for alignment purposes. Static image mode allows storing and displaying a single pattern as the name suggests. HDMI Port mode allows external pattern streaming from the display of the computer however it has the limitation of GPU power and display refresh rate which is typically 60 Hz. Lastly, chip can operate in stored pattern sequence mode. In this mode, 96 images with 1-bit depth can be stored. In this mode trigger settings can be configured which can be either internally done with the set frequency for pattern change or it can be set based on a TTL pulse signal fed to the LightCrafter. The longest period for pattern change is two seconds whereas shortest period was found experimentally, explained in chapter 3.

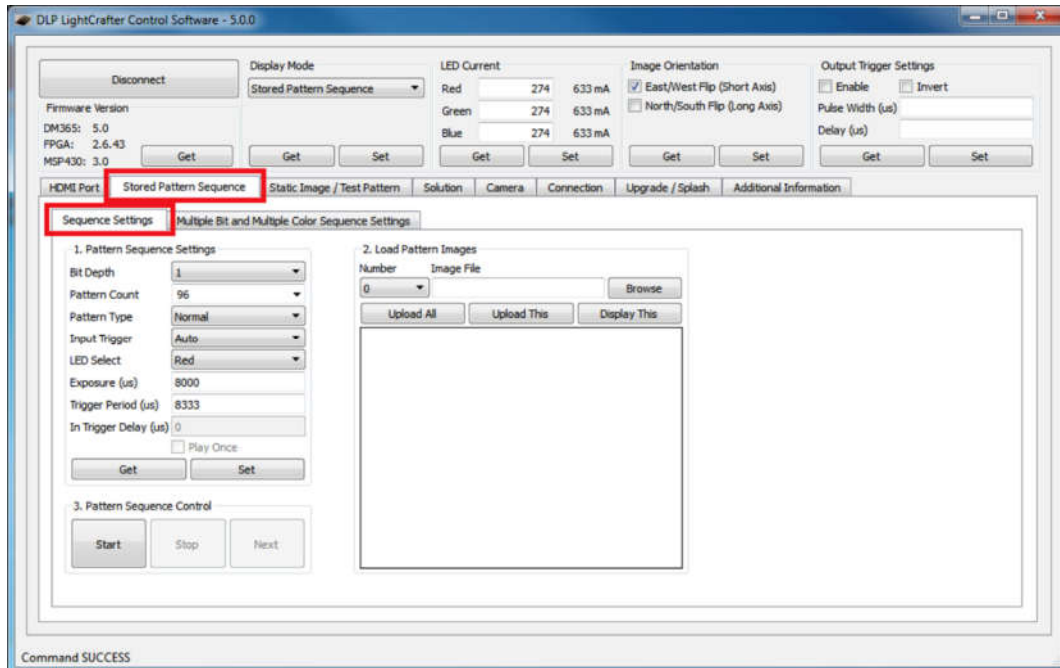


**Figure 2.12 Interface of the LightCrafter Software**



To build an imaging system utilizing DMD chip, light engine of the LightCrafter was removed and chip was exposed. In our studies with DMD chip, a diode laser with wavelength of 532 nm and 20 mW output power was used. It was collimated and expanded so that it would cover the entire chip. After passing the diffuser to reduce speckling and provide uniform illumination[43], LightCrafter was aligned such that when mirrors are in “off” position the reflected light is directed towards optical axis of the microscope to be focused on the image plane. When the mirrors are in “on” position, the reflected beam is strayed to off axis therefore realizing the scanning of the specimen. Results acquired is presented in chapter 3.

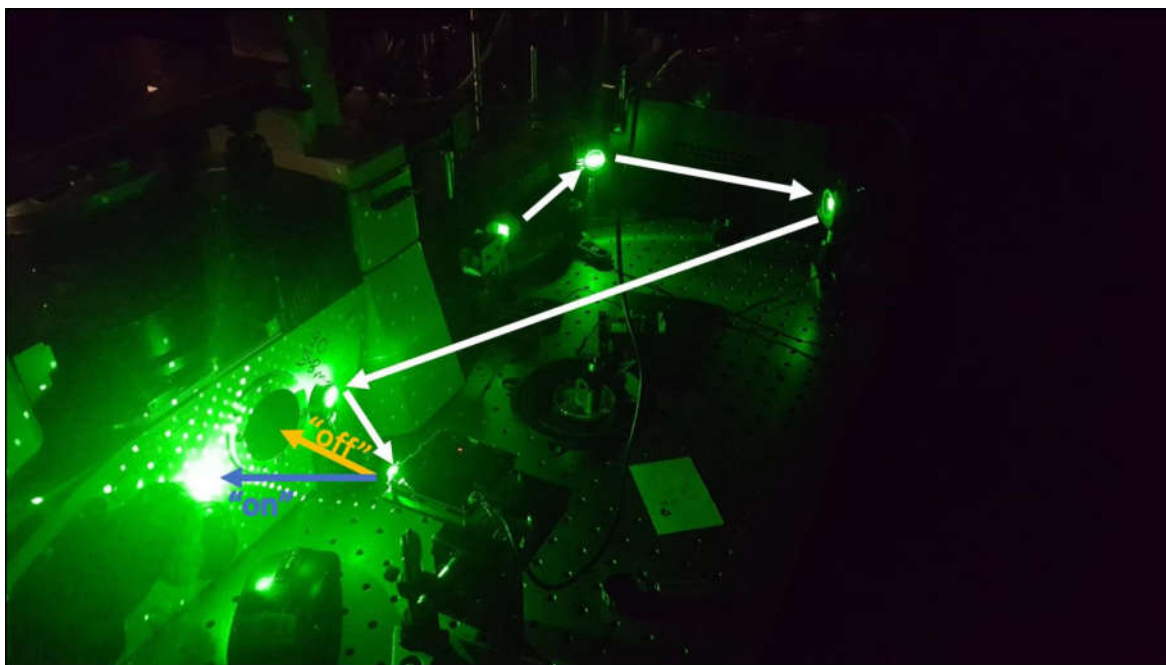


**Figure 2.13 Photograph of the DMD-based Imaging Setup**

## **Chapter 3: Results and Discussion**

### ***3.1 Instrumentation of Galvanometric Optical Scanner Based Confocal Microscope and Obtained Results***

One of the initial things that was done in the context of instrumentation of the Opto-Digital confocal microscope was to design and construct a small voltage supply circuit and its housing to provide potential between 0 and 1.25V to adjust sensitivity of the photo multiplier tube when required. After the soldering, it was sealed in a wooden box and its output was connected to the PMT.



**Figure 3.1 Working and Integration Progress of Potential Supply**

In the previous works involving the instrumentation of the setup, a custom LabVIEW based software was developed[44]. So, I did not have to re-invent the wheel however, a thorough reverse engineering was made to pinpoint the issues initial software had, improve them and implement new features.

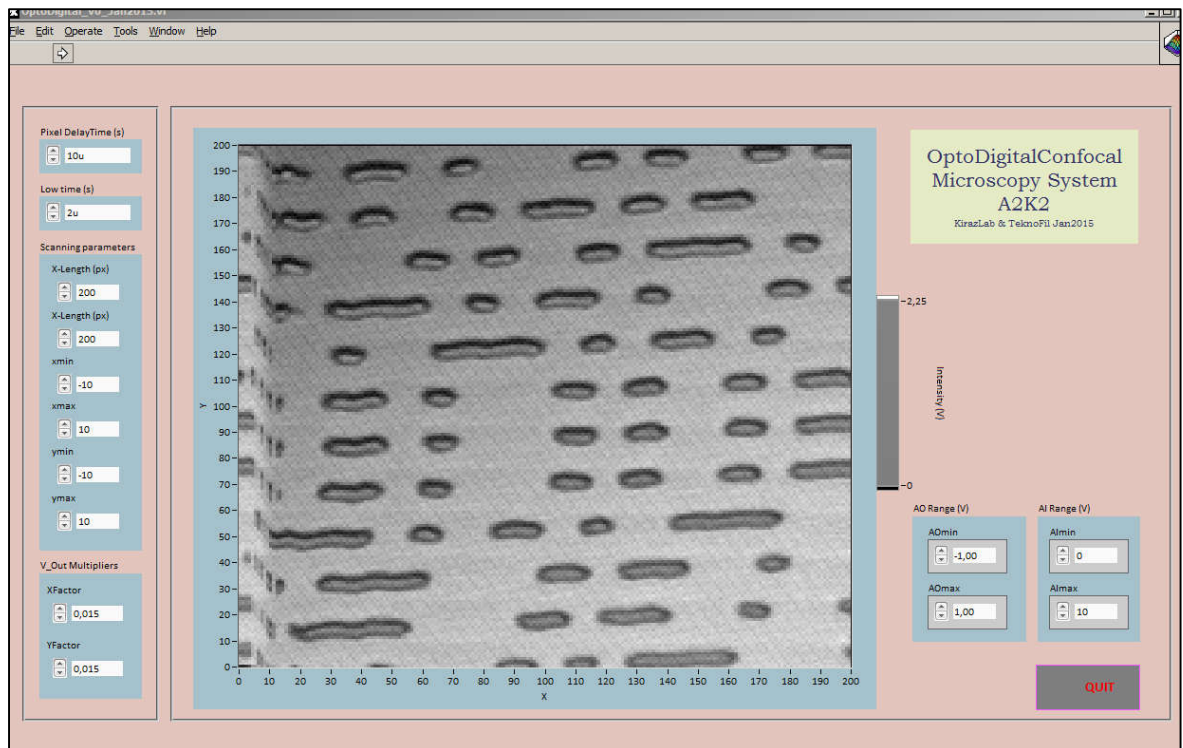


**Figure 3.2 Interface of the Initial Version of A2K2**

By looking at figure x, one can notice two imperfections about the initial software. Firstly, number of inputs in the interface are overwhelming for a person who would want to use the system. As the functions of the inputs lack the explanation, a person who is not developing the software might find using the software as a daunting task. Therefore, the first

aim was to create a more user-friendly software. Secondly, at the left hand-side of the confocal image of cd pattern, distortions can be observed. The reason behind this problem lies in the raster scan algorithm. The initial algorithm worked as following, the x mirror rotates so that beam scans the specimen from left to right and y mirror is rotated at the end of x scanning line. However, this has caused x scan mirror to reset too fast, resulting in distortion in image originated from inertia. Therefore, another aim in the context of development was to optimize scanning algorithm.

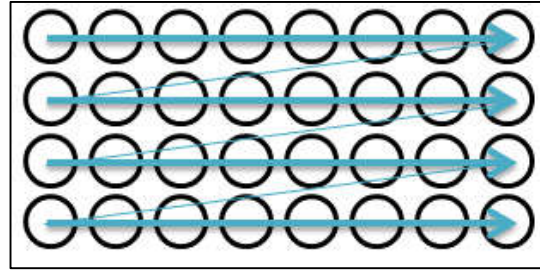


**Figure 3.3 Raster Scan Illustration[48]**

Additionally, features like scanning based on scan area entered by user in the unit of micrometers and having the widefield image from the camera at the backport of microscope simultaneously with the confocal image was planned to be implemented to the software. To breakdown, initial software had 4 sub programs working under the main program. Three can

be seen in main “block diagram” of the software, namely “Init.vi” ( ), “Scan.vi” ( ) & “Close.vi” ( ). Init.vi lies inside a structure called “flat sequence”, which ensures this subprogram runs first and lets out tasks that goes in Scan.vi. Tasks are finally carried to Close.vi where they get cleared to be re-used.

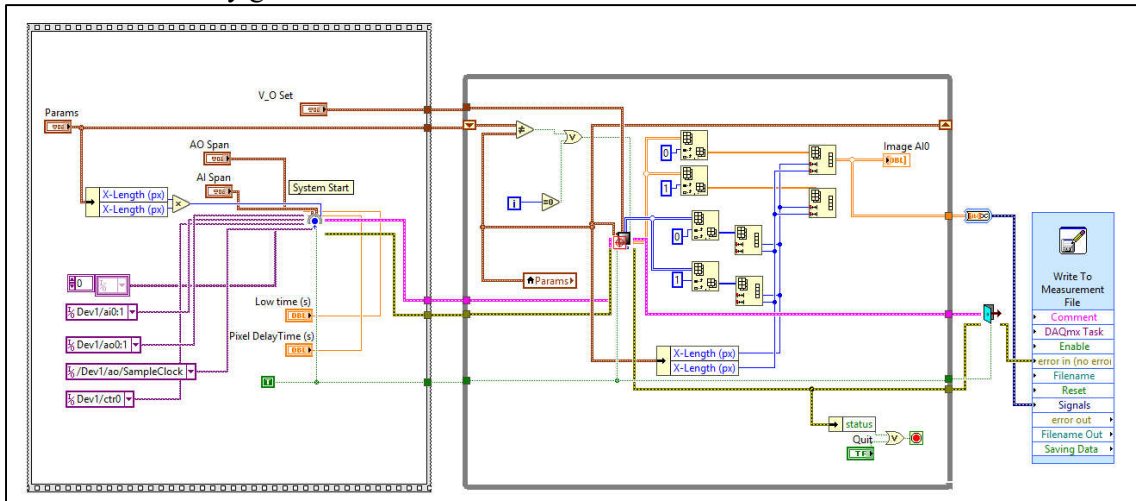


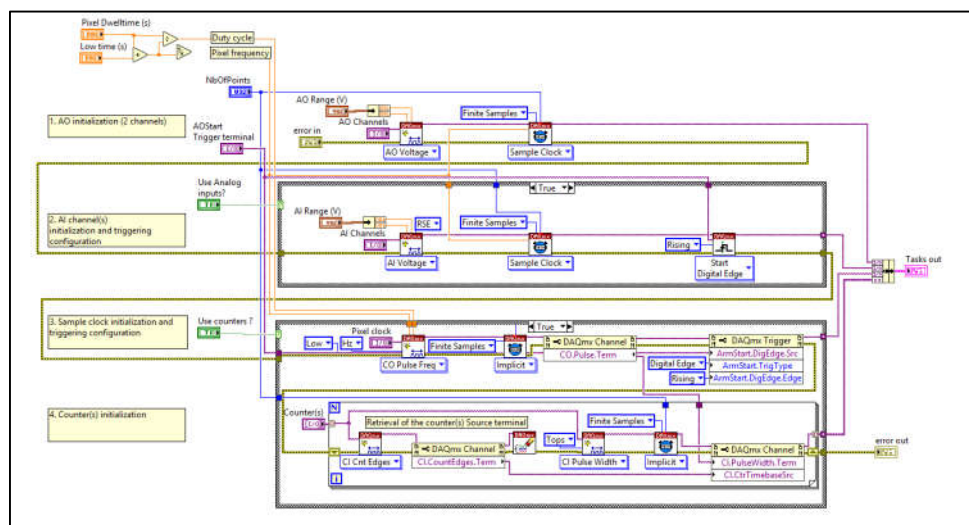
**Figure 3.4 Block Diagram of the Initial Version of A2K2**

In the while loop, Scan.vi contains one another subprogram “RasterScanXY.vi” ( ) where waveform for scanner mirrors is generated.




“Params” and “V\_O Set” clusters contain parameters used both in Init.vi and Scan.vi. In flat sequence “AO Span” and “AI Span” correspond to maximum range for analog output and analog input channels. Also “Dev1/ai0:1” and “Dev1/ao0:1” are the names of available channels to be used on DAQ card. Finally, pixel delay time is the time spent on a single spot before moving to next one and low time defines the time spent between sampling points.

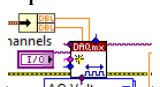
- Init.vi

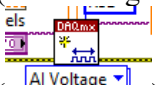


**Figure 3.5 Block Diagram of “Init.vi”[44]**


As mentioned above, addition of pixel dwell time and low time correspond to time between two data points being collected. This information and total number of data points (multiplication of pixel number inputs) are required for “DAQmx Timing (Sample clock).vi”

(). This task sets the type(finite/continuous), amount and rate of data point collection. Rate of data acquisition(frequency) is defined by  $(1 / (\text{dwell time} + \text{low time}))$ . Two channels (Analog Output and Analog Input) are created by “DAQmx Create Channel

(AO-Voltage-Basic).vi” () and “DAQmx Create Channel (AI-Voltage-Basic).vi”

(). Terminal names and voltage values were pre-defined in program.

In order to synchronize data acquisition and scanning, “DAQmx Start Trigger (Digital

Edge).vi”() which ensures Analog Input signal acquisition starts when Analog Output signal generation starts by using sample clock of Analog Output as source. Finally, AI and AO tasks are sent to Scan.vi. The “Init.vi” also contains a counter module but it has not been used.

- Scan.vi

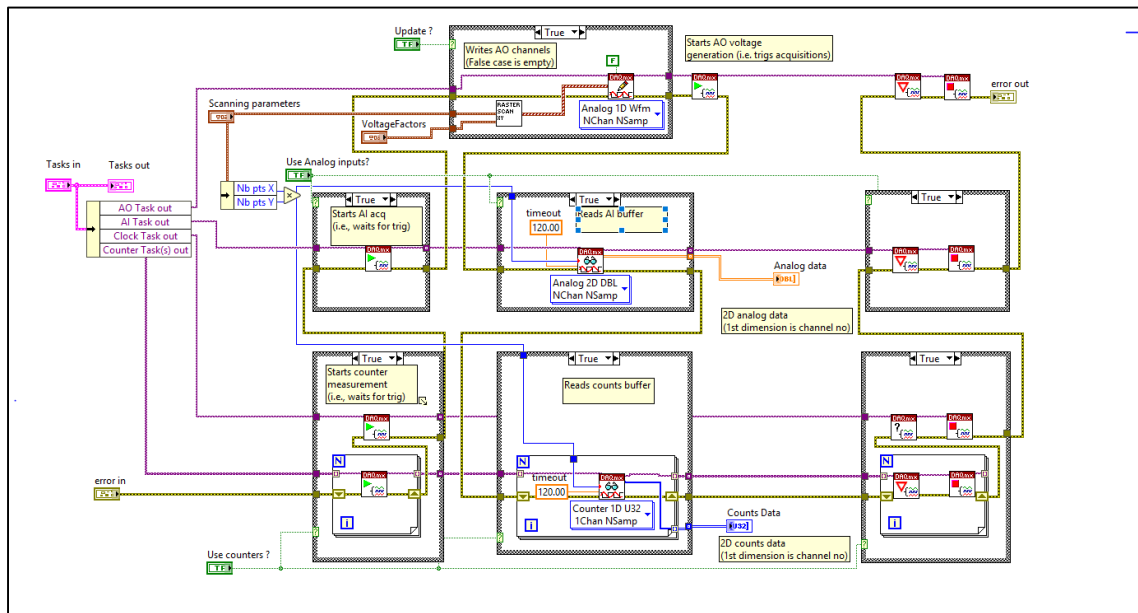


**Figure 3.6 Blockdiagram of “Scan.vi”[44]**

First the out AI Task is sent to “DAQmx Start Task.vi” which waits for output signal to be generated. Here parameters from “Scanning parameters” and “VoltageFactors” clusters are sent to RasterScanXY.vi, which contains pixel numbers, minimum and maximum voltage values to be applied to servo motors. While allowed min. and max. voltages were previously defined, “xmin”, “xmax”, “ymin”, “ymax” allows customizing exact potential to be applied. For example, from -5 to 5V for x and y coordinates.

**Figure 3.7 “Params” Cluster**

Voltage factors cluster simply sets a multiplication factor, for example if the xmin/max and ymin/max are defined from -10V to 10V and voltage factors for x and y are 0.1, then applied voltage to scanner will be between -1V and 1V.

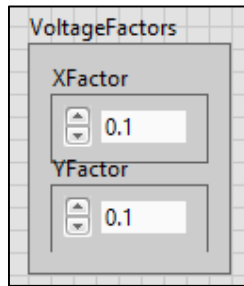
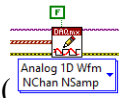
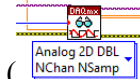


**Figure 3.8 “VoltageFactors” Cluster**

After the waveform is generated in subprogram RasterScanXY.vi, it is sent to “DAQmx



Write (Analog 1D Wfm NChan NSamp).vi” ( ) to be written to analog channels. Then again, task from “DAQmx Write” is sent to “DAQmx Start Task” where analog output signal starts to be sent to scanner mirrors. At the same time, analog input data acquisition starts as sample clock source of this task was set to analog output sample clock.



Then, this task is sent to “DAQmx Read (Analog 2D DBL NChan NSamp).vi” ( ) where data in buffer was being read. Finally, this obtained data (array of AI values) is sent to main program to be arranged and converted to image.

Thus, obtained array is reshaped with dimension based on the number of pixels that was defined in the first place. Lastly, this 2D array of Z values (Analog Input) is converted to intensity graph.

When user exits from program saving window pops up to write the measurement to a file.

- *RasterScanXY.vi*

Produces the following waveform to be applied to the galvanometer scanner mirrors.

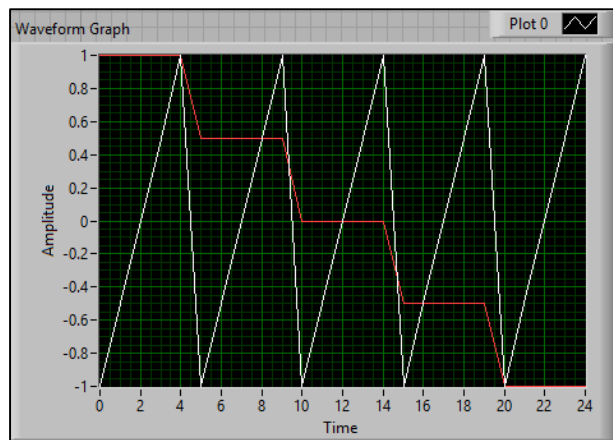


**Figure 3.9 Waveform Graph of the Applied Potential to the Scanner Mirrors**

- Close.vi

As program runs continuously, channels need to be cleared for using in repetition. Every single generated task is sent to “DAQmx Clear Task.vi” ( ).

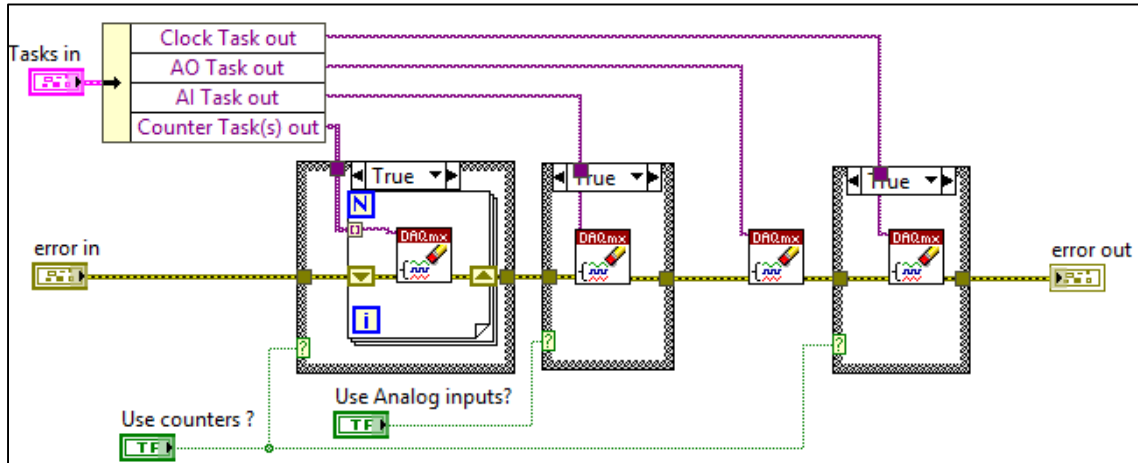


**Figure 3.10 Block Diagram of the “Close.vi”[44]**

Firstly, to give a friendlier feeling to the user the interface was reworked. A combobox namely “scan speed” was created with pre-defined speeds by combining “low time” and “pixel delay time” inputs together. The “fast” choice of imaging takes time of  $5\mu\text{s}$  between two-pixel points whereas “normal” takes time of  $10\mu\text{s}$  and “slow” setting takes  $20\mu\text{s}$ . Similarly, the pixel numbers were again pre-defined in a combobox. By measuring the distance between stripes of calibration ruler for applied voltages to scanner mirrors the conversion number from applied voltage to distance in image plane was found and scan area inputs are implemented accordingly. These three selections constitute the scan parameters of the software and required changes in the block diagram was made respectively.

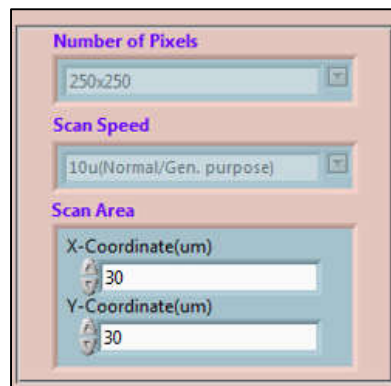


**Figure 3.11 Scan Parameters of Revised Version of Software**

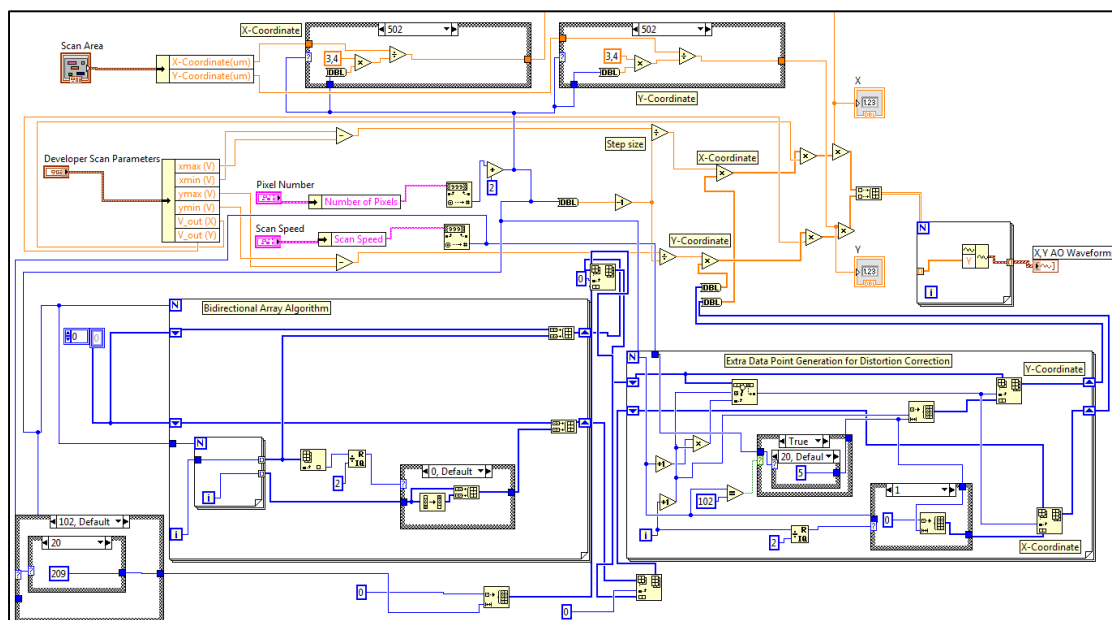
Next was to implementation of developer mode and widefield camera image. Starting off with the developer mode, there are crucial parameters such as maximum allowed potential that can be applied to scanning mirrors which may require access during the development

process. Thus, once the program was running with the toggle switch “developer mode” on, these parameters become apparent in the interface with a small piece of warning. Obtaining the widefield image in software was possible with the accessible .NET library in LabVIEW, provided by the supplier. As the program runs, it was possible to activate camera by initialization and start capturing, where live mode could be stopped any time during runtime.



**Figure 3.12 Developer Scan Parameters and Widefield Imaging**

To optimize the scanning algorithm, scanning sub program “rasterscan.vi” was written from scratch. The idea was to apply a waveform to mirrors in a manner that scanning was to be made “bi-directional”, eliminating the inertia caused distortion in the confocal images. In this context the written program and waveform it produces and the block diagram of the program is demonstrated in the figure below.



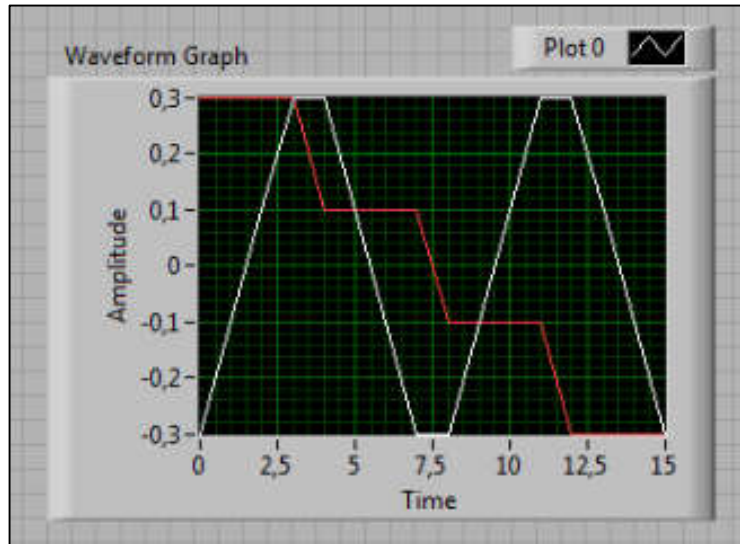


**Figure 3.13 Block Diagram of Bidirectional Algorithm and Produced Waveform**

The program produces the theoretically desired waveform and successfully performing bidirectional scanning on the specimen, yet the resulting images had another type of distortion, namely “ghosting”.

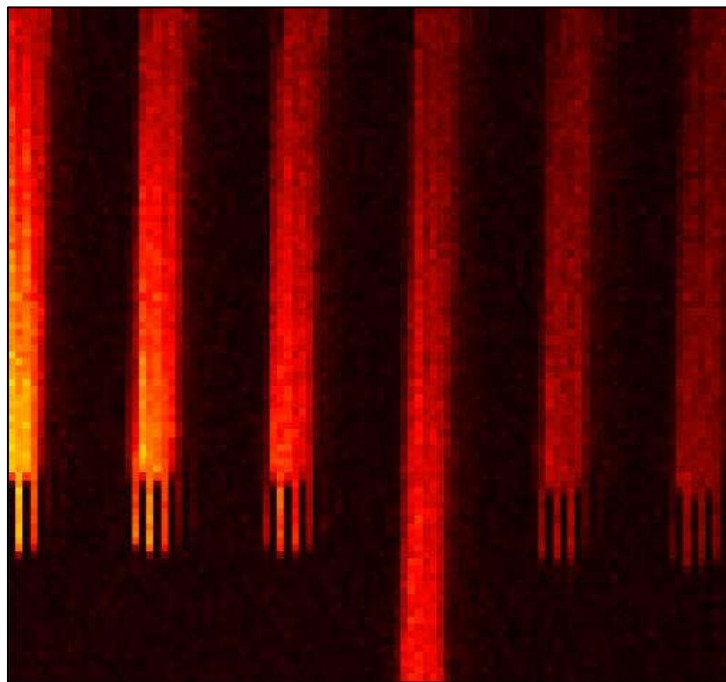


**Figure 3.14 Image of Microruler with Ghosting Distortion, Pixel Number = 100x100 Pixels**

Although sub-optimal, ghosting distortions in the confocal images were eliminated by getting rid of some of the initial data points in other words certain number of pixels. For every scan speed and number of pixels, ideal number of pixels to be added and then



subtracted at the beginning of the scan when forming the image was found empirically. In a series of attempts to improve the program cumulatively added up to final interface given in the figure below. The program achieves 1 frame per second confocal image generation for pixel number of 500 x 500 pixels, 60  $\mu\text{m}$  x 60  $\mu\text{m}$  scan area and “normal” scan speed.

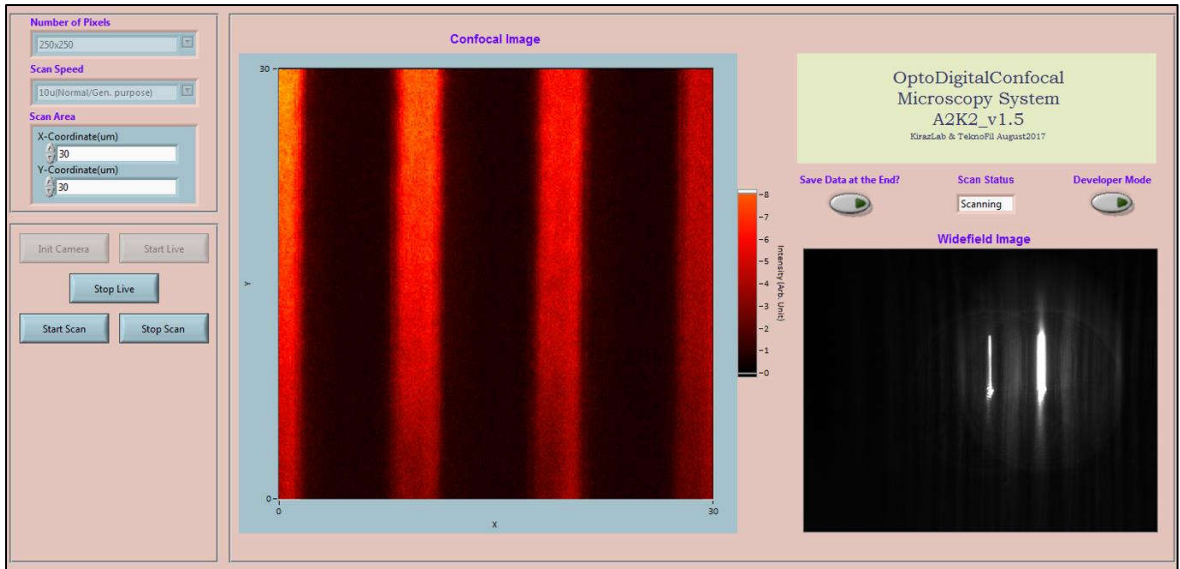


**Figure 3.15 Interface of the Improved Software**

Block diagram of the main program is presented below.

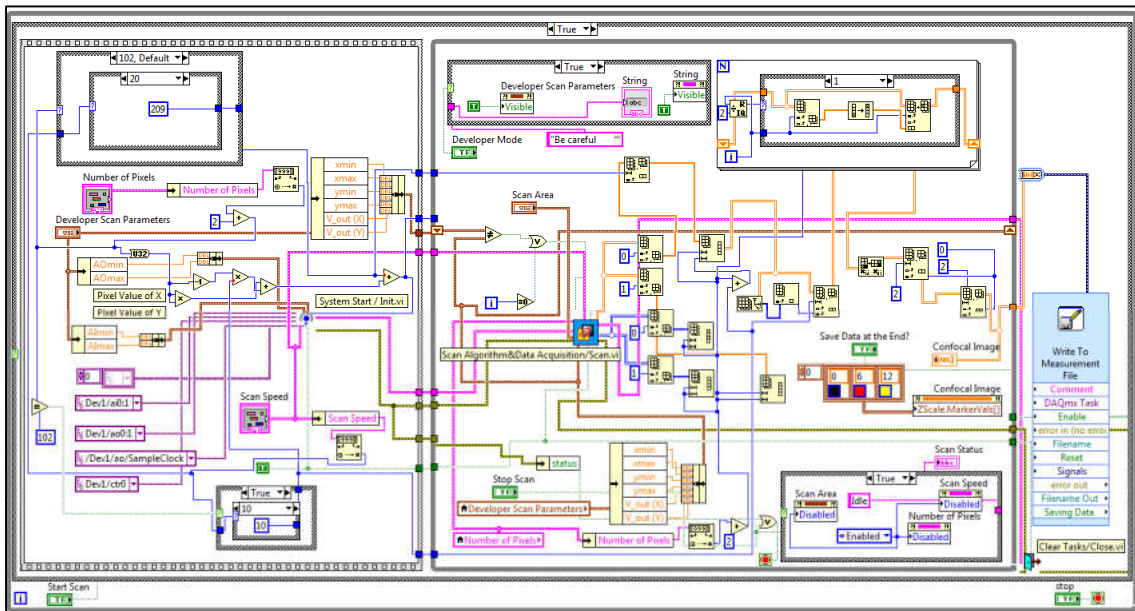


**Figure 3.16 Block Diagram of A2K2 v1.5**

The resulted images of calibration samples are given below.

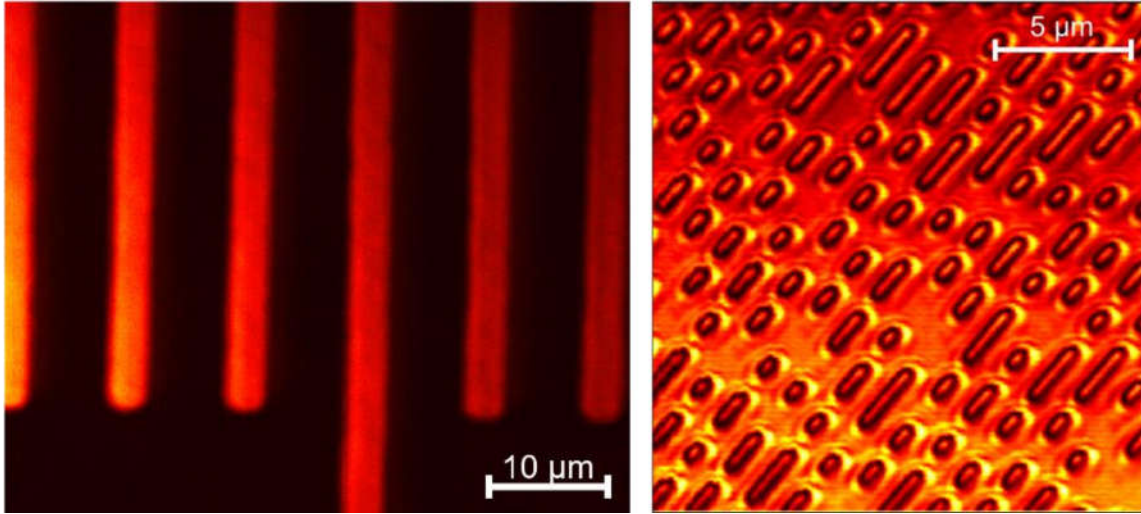


**Figure 3.17 Confocal Images of Microruler and Cd-Pattern, Pixel Number = 1000 x 1000 Pixels**

### 3.2 Results Obtained with DMD-Based Optical Scanner

As an alternative for light steering and investigating the image quality, DMD based imaging setup was built. Microruler was used in our investigations with the DMD as imaging sample. One of the first tasks was to identify maximum frequency that chip reaches between displaying two images. To do so, two images were uploaded to LightCrafter and displayed in image sequence mode. The trigger mode was activated where as an input a pulse signal with 3.3V, 50% duty cycle was fed to the LightCrafter. The reflected beam was directed to a silicon photodetector and its output was connected to oscilloscope. The maximum transition frequency between images in sequence was found to be 4.4 kHz.

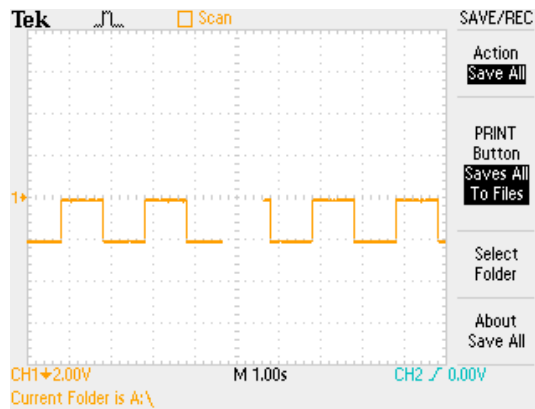


**Figure 3.18 Oscilloscope Data of LightCrafter Operating in Image Sequence Mode with 1 Hz Frequency**

The LightCrafter consists of 608 x 684 mirrors on its DMD chip and uploaded images can be displayed in sequence in image sequence mode. Unfortunately, it is limited to store 1-bit 96 images, therefore it was required to create scanning algorithms that produces 1-bit 96



images which covers the entire mirrors to complete scanning. To do so, two scanning algorithms were developed. One is called “single spot scanner” whereas the name suggests a single spot of 0 valued (“off” position) rectangular moves around in the 608 x 684 pixel image. As the 96 images is generated, the entire 608 x 684 pixel image’s scanning was complete.

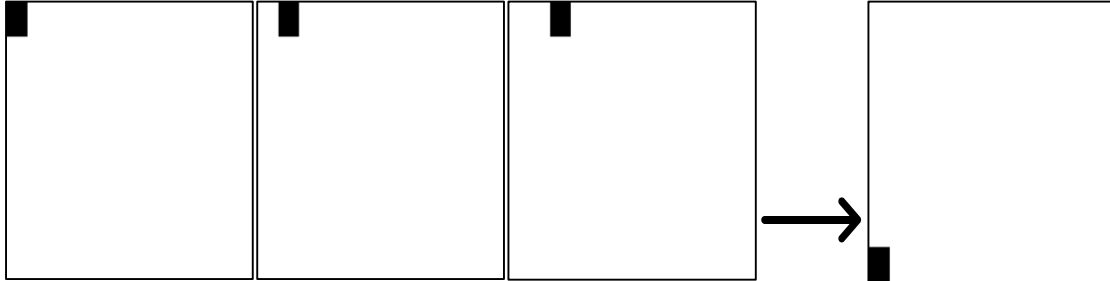


**Figure 3.19 Produced Images of Single-spot Scanning Algorithm**

As an alternative to scanning algorithm, “Multi-spot scanner” was developed. In this algorithm, produced images consist of multiple single pixels that are being moved around, again covering the whole area of 608 x 684 image matrix.

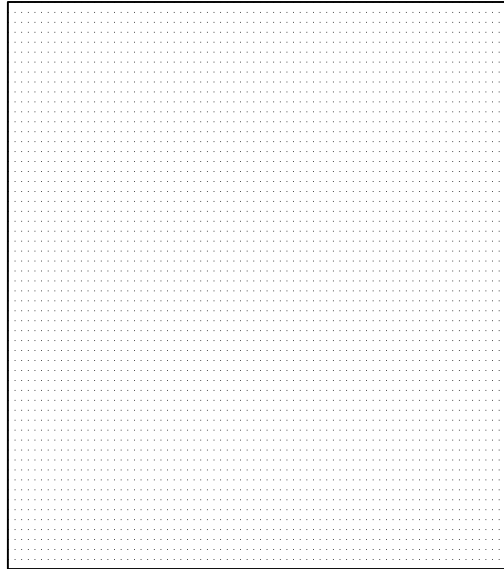


**Figure 3.20 Example Image of a Multi-spot Scanning Algorithm. Produced 96 Images Cover the Entire Array of Mirrors.**

In addition to comparison of usage different scan algorithms, diffuser with its position in space being stationary or moving are compared in the obtained images. To realize movement of diffuser, it was placed on a speaker, which was driven with a sinusoidal wave of 5 Hz and 3 V peak to peak amplitude. However, the displacement of the diffuser was not enough, so the output signal of the function generator was connected to an amplifier (Falco Systems WMA-300) which provided the required amount of displacement by amplifying the current driven to the speaker. In the figure below images of microruler without diffuser and

with diffuser for two objectives. For the air objective, effect of the diffuser movement becomes more apparent.

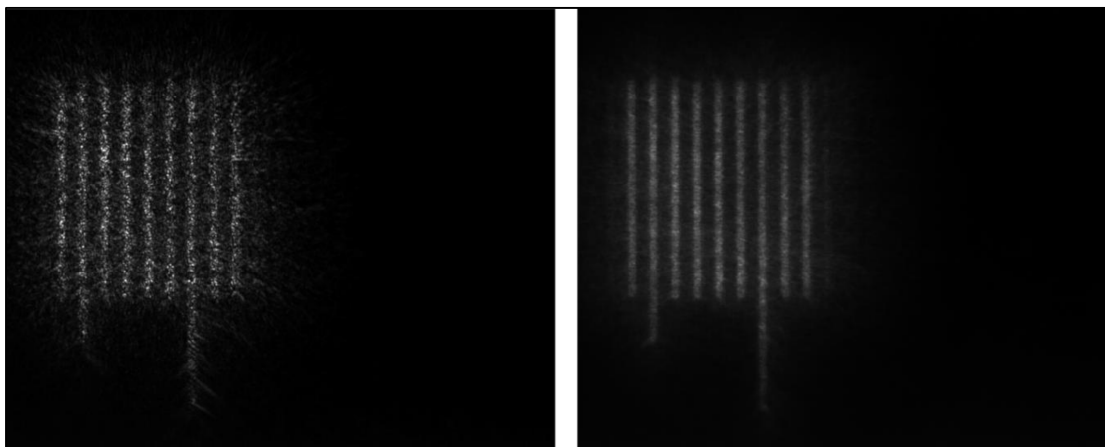


**Figure 3.21 Comparison of Images with Diffuser Being Stationary and in Movement, 40x 0.55NA Air Objective, All Mirror on “off” Position.**

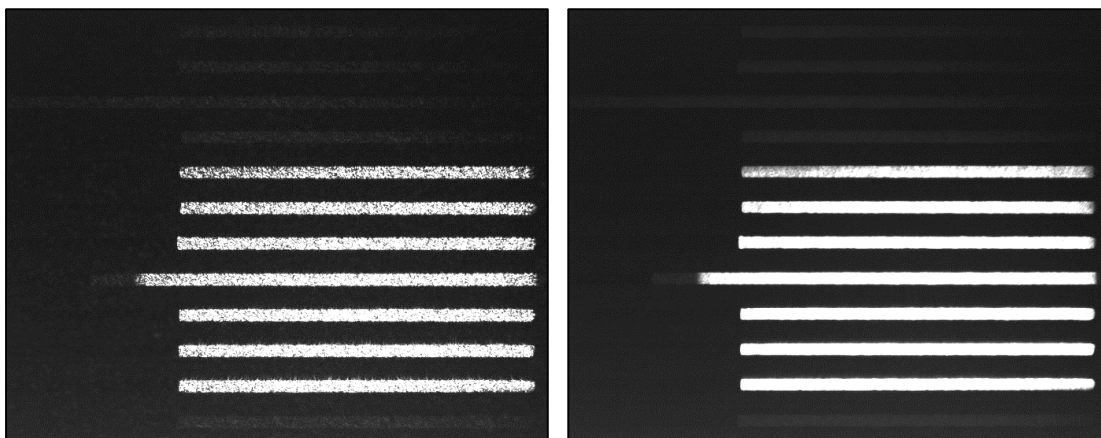


**Figure 3.22 Comparison of Images with Diffuser Being Stationary and in Movement, 60x 1.49NA Air Objective, All Mirror on “off” Position.**

For diffuser moving and DMD scanning the sample with images produced by single-spot algorithm, result is given below.

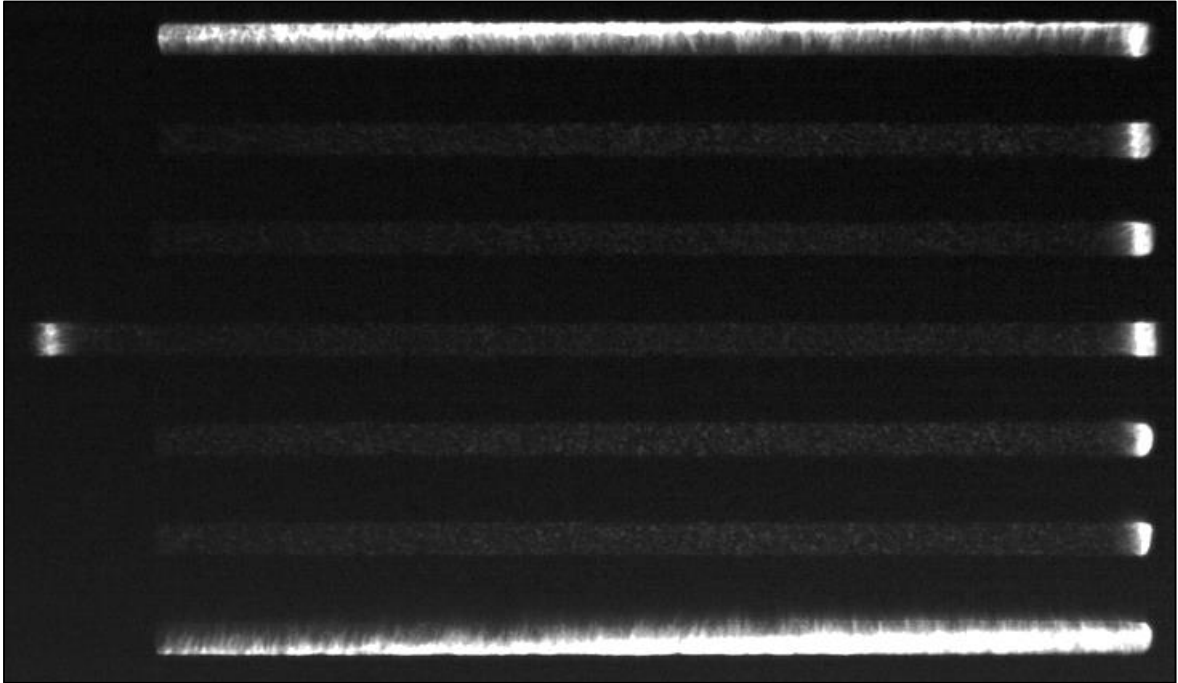


**Figure 3.23 Single-spot Scanning of Microruler, 4.4 kHz Scanning Frequency**

Imaging results of the same area with all mirror on, single-spot scanning and multi-spot scanning are given below.

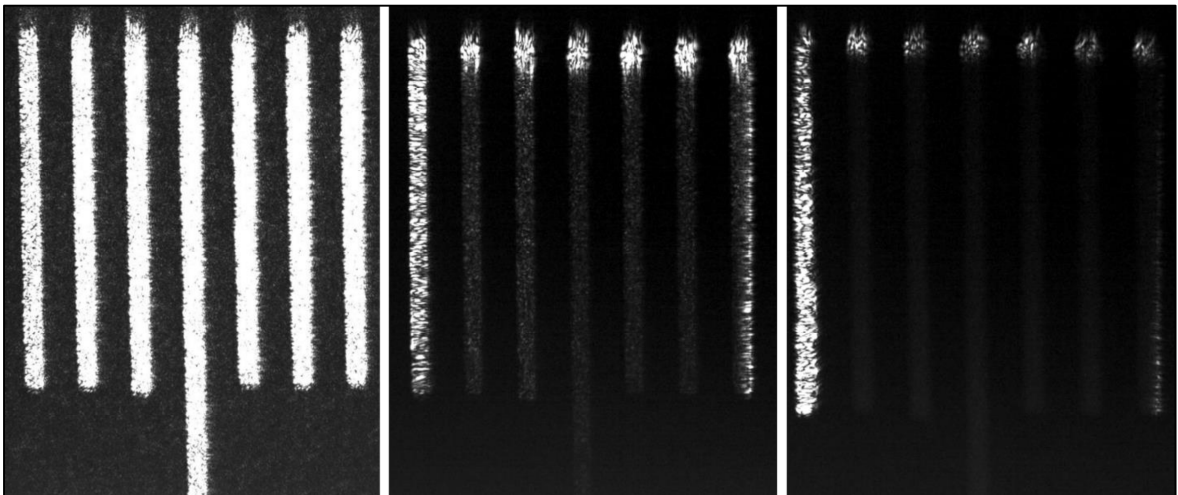


**Figure 3.24 Diffuser in Movement and 4 kHz Scan Speed. All Mirror Off, Single-Spot Scanning and Multi-spot Scanning Results.**

As it can be seen in Figure 3.24, using scanning algorithms reduces the background noise in the image. In addition, image obtained with the multi-spot algorithm has less intensity variance along the microruler stripes however, it has relatively low intensity. To further enhance the image quality improvement over widefield imaging with DMD scanning, a LabVIEW program was developed for programming of the camera. The idea was using the triggering of camera with the output trigger signal coming from the LightCrafter so that

images in sequence would be saved in synchronization with the DMD-based scanning. The output triggering signal of LightCrafter is a 3.3V pulse train, however the camera required a minimum of 5V square wave to be triggered. Therefore, a current source follower circuit was developed and its output was connected to the camera.

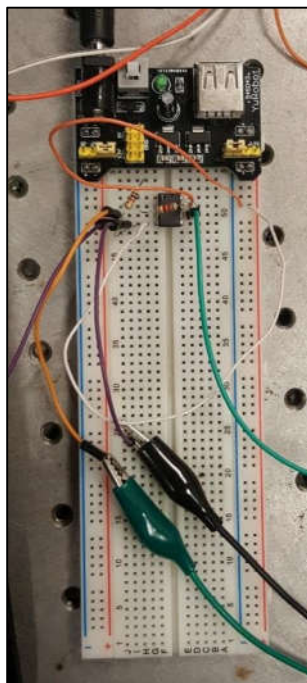


**Figure 3.25 Current Source Follower Circuit**

The developed program uses .NET library references provided by the manufacturer and produces analog input signal that is meant to be fed to trigger input of DMD. Then output trigger signal from LightCrafter is sent to the camera, where for every rising edge of the incoming pulse, an image is saved. Once the program starts the run, it waits until the camera receives initial signal. The downside of this type of operation is scan period for each image is limited to 1 second, as this is the minimum amount of required time for the camera to receive the signal, display and save image. The work was carried out using images produced by single-spot scanning algorithm.

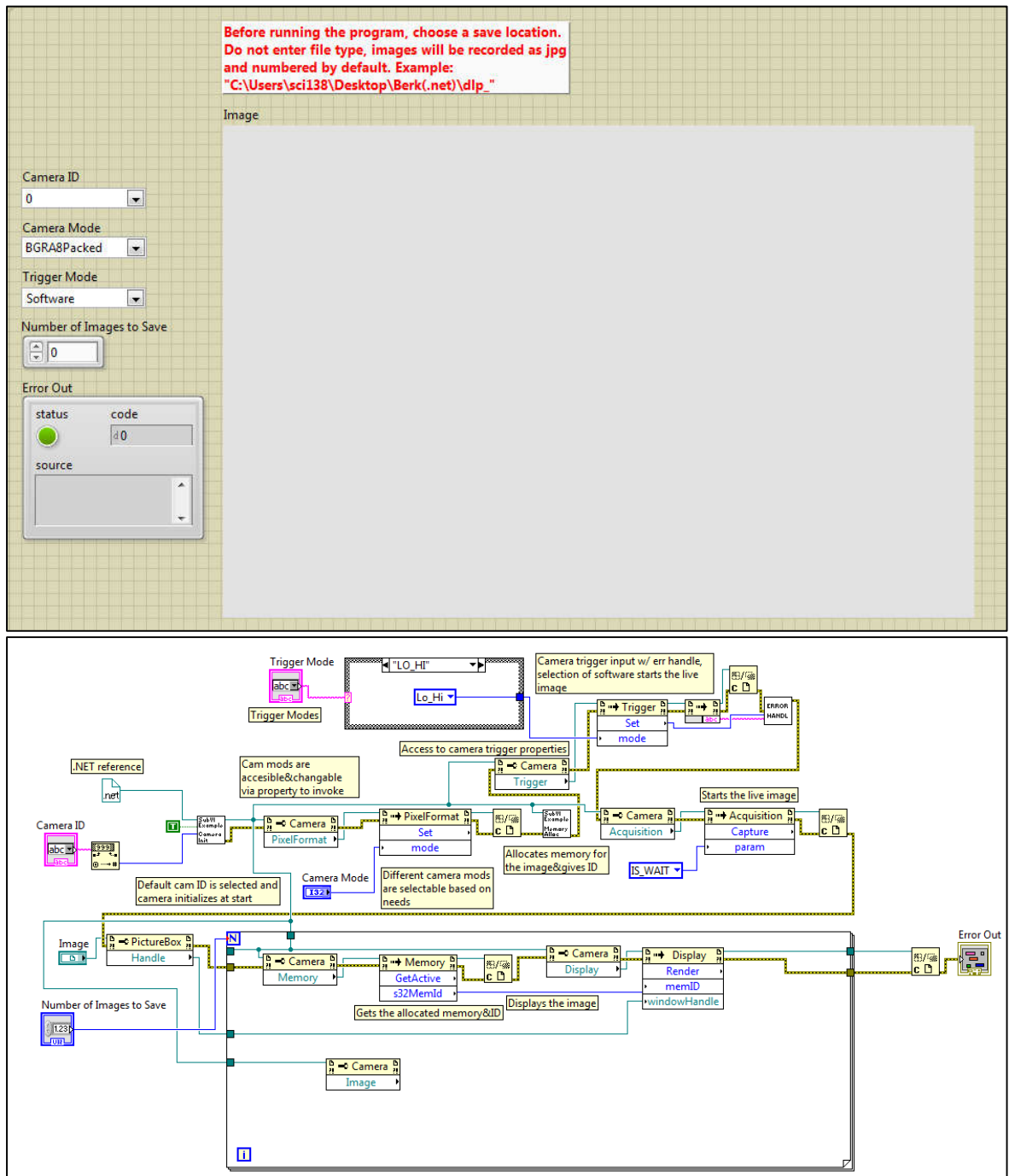


**Figure 3.26 Interface and Block Diagram of Camera Triggering Program**

Recorded 96 images for each scanning are then stitched together and improved by means of applying digital filtering. The trade-off in this method of imaging is requirement of 96 seconds of scanning and saving of images to be completed and post-processing. Stitched and processed images were recorded with low NA air objective.

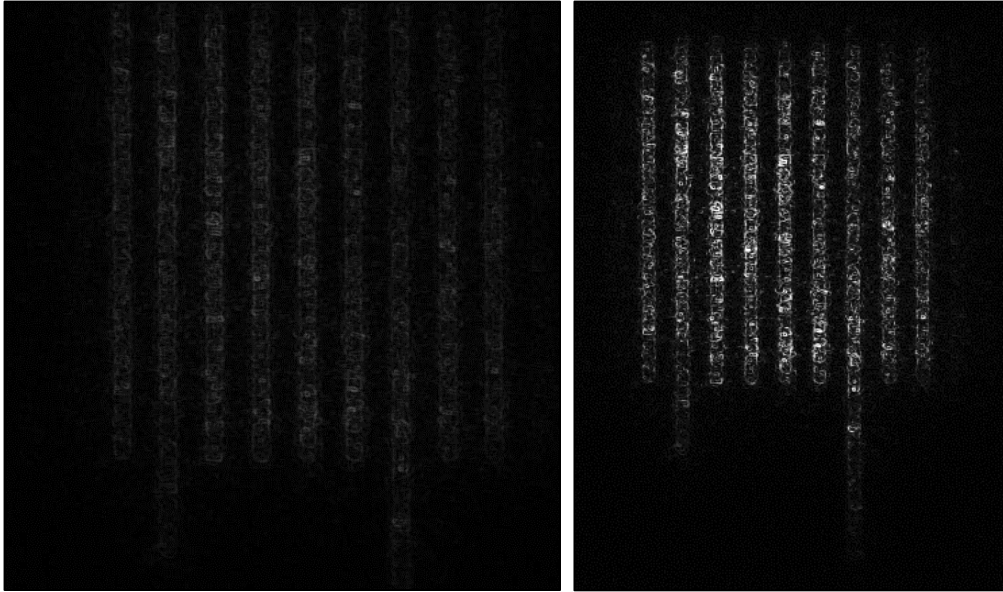


**Figure 3.27 Post-processed Image Result with Range Filter on Left Hand Side and Standard Filter Result on Right Hand Side**

Analysis of the obtained images are given below, intensity profiles along a line on microruler in 8-bit values to pixel coordinates graph was obtained and signal to noise ratios were calculated respectively[45].

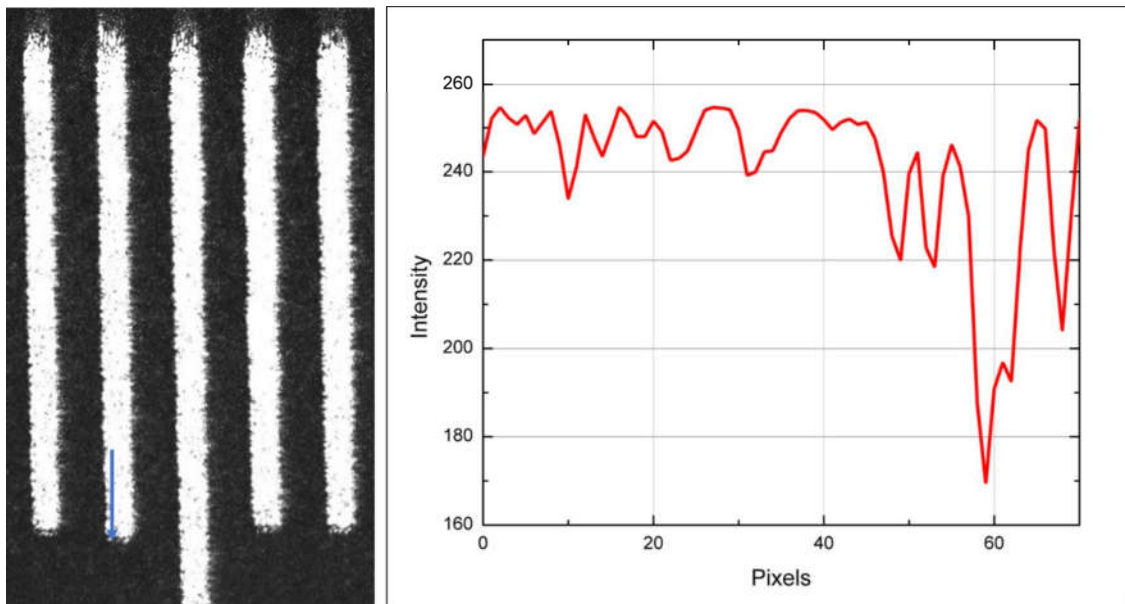


**Figure 3.28 Image Obtained with All Mirrors in Off Position and Intensity Profile along the Chosen Line. (Mean = 239.62, Standard Deviation = 19.87, Signal to Noise Ratio = 12.05)**

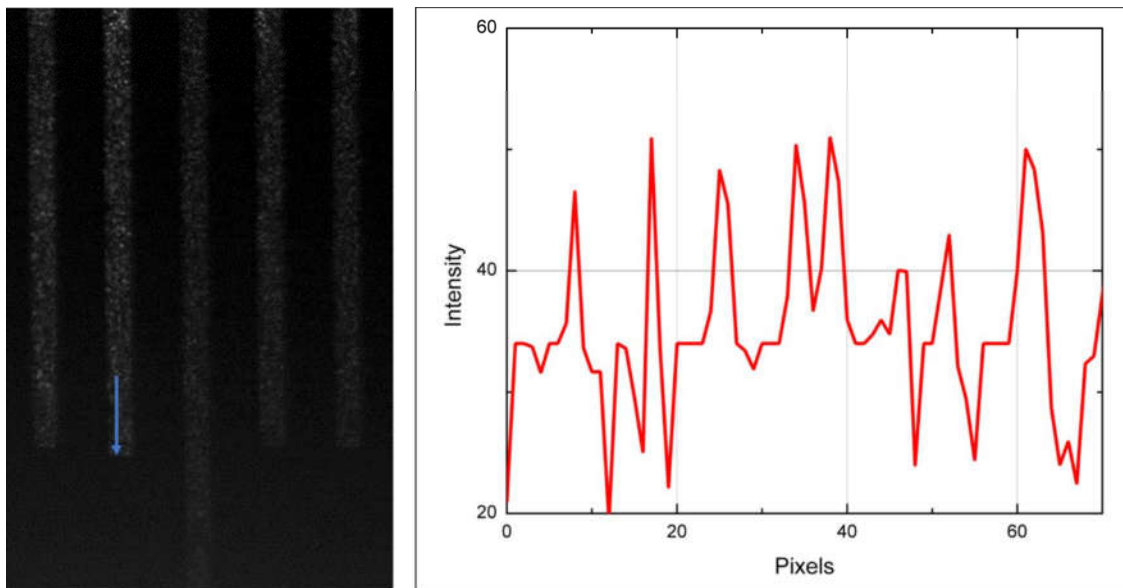


**Figure 3.29** Image Obtained with Single Spot Scanning and Intensity Profile along the Chosen Line. (Mean = 35.27, Standard Deviation = 7.16, Signal to Noise Ratio = 4.92)

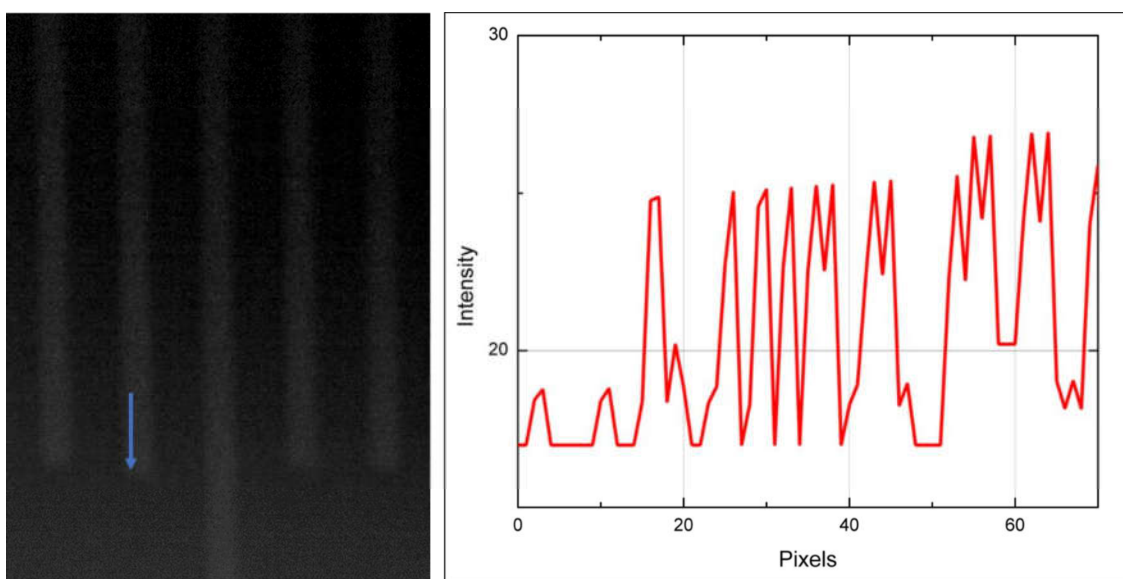


**Figure 3.30** Image Obtained with Multi Spot Scanning and Intensity Profile along the Chosen Line. (Mean = 21.56, Standard Deviation = 4.03, Signal to Noise Ratio = 5.34)



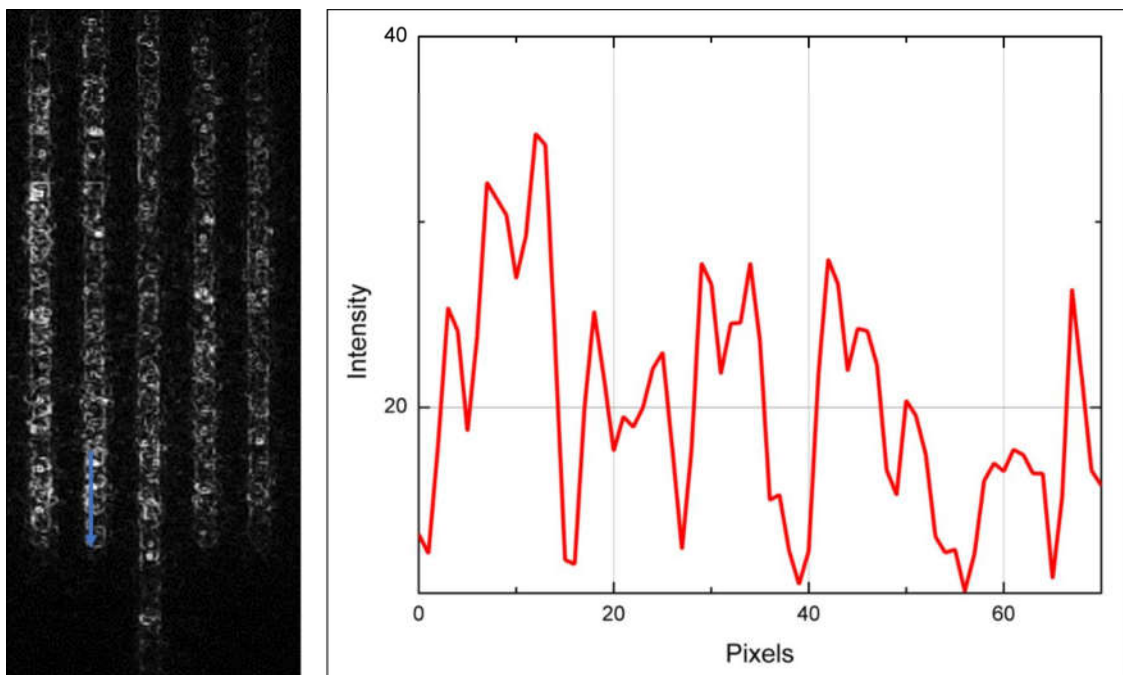


**Figure 3.31 Image Obtained with Multi Spot Scanning and Intensity Profile along the Chosen Line. (Mean = 20.01, Standard Deviation = 6.12, Signal to Noise Ratio = 3.26)**

## Chapter 4: Conclusion

In this work, two optical setups were built. The first setup was a custom laser scanning confocal microscope. Setup was built around an inverted microscope, employing 488 nm wavelength with 5 mW output power, galvanometer scanner mirrors, a scan lens, camera, beamsplitter and a photon multiplier tube. The setup had a prior LabVIEW based software with room to improve. First improvement done in the setup was building a potential supply that varies between 0 and 1.25V to adjust sensitivity of the PMT. After that, interface of the software got reworked by means of simplification for whom not familiar with development. In addition, raster scan algorithm was developed from scratch. The new scanning subprogram employed a bidirectional scanning algorithm to evade distortions formerly present. In a sense, new scanning program did correct the previous distortions in obtained confocal images emerging from inertia of x-mirror due to fast reset. However, it has introduced another type of distortion namely “ghosting”. This distortion has appeared to stem from synchronization although data acquisition and mirror scanning starts at the same time in the software. To get rid of ghosting, certain number of pixels were added for each scan speed and pixel number setting, that were then made redundant and removed from final image. This empirical solution was a success in terms of distortion correction and even though it introduces additional pixels that are not used in final image, it was possible to get 1 frame per second confocal image speed for 60  $\mu\text{m}$  x 60  $\mu\text{m}$  scan area, 500x500 pixel number and “normal” scan speed. Calibration samples were confocally imaged and presented. The software still got plenty of space to improve, including a better solution to scanning algorithm, analysis features, sectioning capabilities for 3D reconstruction of the specimens.

Additionally, another optical scanner namely the DMD chip on LightCrafter from Texas Instruments was used in confocal configuration. To obtain images utilizing the DMD chip, CMOS camera at the backport of the microscope was used. To realize scanning, two scanning algorithms were developed that produces 96 1-bit images ensuring all the mirrors on the chip are activated. Before the LightCrafter, a diffuser was placed to reduce speckling in image by providing a uniform illumination on the chip. It was made to move in space while scanning and obtained results in both situations were compared. The maximum frequency between images in sequence passing was found to be 4.4 kHz. Highest signal to noise ratio was obtained while all mirrors were in off position. However, speckling at the boundaries of the microruler can be observed. These distortions were removed by utilizing scanning algorithms. Although multi spot scanning yields slightly higher signal to noise ratio compared to single spot scanning, higher levels of light intensity are required for better results as the mean value indicates. Then, to further enhance image quality post-processing was used. To do so, the LightCrafter’s trigger output signal was connected to the camera’s trigger input and a LabVIEW based program was developed. The pitfall of this method was the speed, as the whole scanning and image saving was possible with 1 image per second. Also, the additional time required for post-processing was another downside. As post-process was achieved by programming the camera, there’s still improvement needed for optimization of post process indicated by the signal to noise ratio. In addition, further work can be done on the setup to get image from reflected light off from the chip using a CCD camera or a point detector.

In conclusion, two laser scanning setups around an inverted microscope were built and operated. For the traditional laser scanning confocal microscopy setup, a custom user-friendly LabVIEW software was developed. For the confocal configuration utilizing DMD optical scanner, different scan algorithms and post processed results obtained with custom camera program were compared.

## References

- [1] G. Gasson, “The oldest lens in the world: a critical study of the Layard lens”. “The Ophthalmic Optician”, 9 December 1972, 1267-72;
- [2] (n.d.) <https://en.wikipedia.org/wiki/Magnification>
- [3] (n.d.) <http://microscopy.berkeley.edu/courses/TLM/cmpd/cmpd.html>
- [4] (n.d.) [http://assets.newport.com/webdocuments-en/images/how\\_to\\_build\\_a\\_beam\\_expander\\_5.pdf](http://assets.newport.com/webdocuments-en/images/how_to_build_a_beam_expander_5.pdf)
- [5] (n.d.) <https://micro.magnet.fsu.edu/primer/museum/hooke.html>
- [6] (n.d.) [https://en.wikipedia.org/wiki/Critical\\_illumination](https://en.wikipedia.org/wiki/Critical_illumination)
- [7] (n.d.) [https://www.keyence.com/ss/products/microscope/glossary/cat5/transmitted\\_illumination/index.jsp](https://www.keyence.com/ss/products/microscope/glossary/cat5/transmitted_illumination/index.jsp)
- [8] M. Locquin, M. Langeron, “Handbook of Microscopy”, 1983
- [9] X. Huang, M.A. El-Sayed, “Gold nanoparticles: Optical properties and implementations in cancer diagnosis and photothermal therapy”, “Journal of Advanced Research (2010) 1”, 13-28, doi:10.1016/j.jare.2010.02.002
- [10] (n.d.) <https://www.nikon.com/products/microscope-solutions/explore/microscope-abc/illumination/index.htm>
- [11] (n.d.) <http://www.icbl.hw.ac.uk/learnem/doitpoms/OpticalMicroscopy/resolution.htm>
- [12] M.Müller, “Introduction to Confocal Microscopy”, 2006
- [13] S. T. Ross, J. R. Allen, M. W. Davidson, “Chapter 2: Practical considerations of objective lenses for application in cell biology”, “Methods in Cell Biology”, Volume 123, 2014, 19-34
- [14] (n.d.) [https://www.microscopeworld.com/t-infinity\\_corrected\\_optics.aspx](https://www.microscopeworld.com/t-infinity_corrected_optics.aspx)
- [15] (n.d.) [http://microscopy.berkeley.edu/courses/tlm/fluor/fluor\\_micro.html](http://microscopy.berkeley.edu/courses/tlm/fluor/fluor_micro.html)
- [16] E. Abbe, Beiträge zur theorie des mikroskops und der mikroskopischen wahrnehmung. Archiv für Mikroskopische Anatomie, 9:413–418, 1873. 10.1007/BF02956173
- [17] O. Schulz, M. Koenig, “STED Microscopy Made Easy”, Biophotonics, Dec. 2014
- [18] S.W. Hell and J. Wichmann (1994). Breaking the diffraction resolution limit by stimulated emission: stimulated-emission-depletion fluorescence microscopy. Opt Lett, Vol. 19, pp. 780-782.
- [19] (n.d.) [https://en.wikipedia.org/wiki/Confocal\\_microscopy](https://en.wikipedia.org/wiki/Confocal_microscopy)

- [20] Hecht, Eugene, Optics, 2nd Ed, Addison Wesley, 1987
- [21] (n.d.) <https://www.olympus-lifescience.com/en/microscope-resource/primer/techniques/confocal/confocalintro/>
- [22] (2006) [http://elm-chan.org/works/vlp/report\\_e.html](http://elm-chan.org/works/vlp/report_e.html)
- [23] (n.d.) <http://in.bgu.ac.il/en/iki/Pages/Spining-disc-confocal-microscopy.aspx>
- [24] Art J. (2006) Photon Detectors for Confocal Microscopy. In: Pawley J. (eds) Handbook Of Biological Confocal Microscopy. Springer, Boston, MA, [https://doi.org/10.1007/978-0-387-45524-2\\_12](https://doi.org/10.1007/978-0-387-45524-2_12)
- [25] Hamamatsu Photonics, “Photomultiplier Tubes Basics and Applications”, (2007)
- [26] (n.d.) [https://en.wikipedia.org/wiki/Digital\\_micromirror\\_device](https://en.wikipedia.org/wiki/Digital_micromirror_device)
- [27] B. Lee, “Introduction to  $\pm 12$  Degree Orthogonal Digital Micromirror Devices (DMDs)”, “DLPA008B-July 2008-Revised February 2018”
- [28] J. M. Younse, "Projection display systems based on the Digital Micromirror Device (DMD)", Proc. SPIE 2641, Microelectronic Structures and Microelectromechanical Devices for Optical Processing and Multimedia Applications, (13 September 1995); doi: 10.1117/12.220943; <https://doi.org/10.1117/12.220943>
- [29] Dong-Hee Lee, “Optical System with 4  $\mu\text{m}$  Resolution for Maskless Lithography Using Digital Micromirror Devices”, Journal of the Optical Society of Korea, Vol. 14, No. 3, September 2010, pp. 266-276
- [30] T. Arens-Arad, N. Farah, S. Ben-Yaish, A. Zlotnik, Z. Zalevsky, and Y. Mandel, “Head mounted DMD based projection system for natural and prosthetic visual stimulation in freely moving rats”, Sci. Rep. 6, 4 (2016).
- [31] Wang, D & Wei, S. (2007). Phase modulation properties of digital micromirror device. Guangxue Xuebao/Acta Optica Sinica. 27. 1255-1260.
- [32] D. Dan, M. Lei, B. Yao, W. Wang, M. Winterhalder, A. Zumbusch, Y. Qi, L. Xia, S. Yan, Y. Yang, P. Gao, T. Ye, and W. Zhao, Sci. Rep. 3, 1 (2013).
- [33] Renjie Zhou, "DMD-based quantitative phase microscopy and optical diffraction tomography", Proc. SPIE 10546, Emerging Digital Micromirror Device Based Systems and Applications X, 105460E (22 February 2018); doi: 10.1117/12.2289163;
- [34] G. Gauthier, I. Lenton, N. M. Parry, M. Baker, M. J. Davis, H. Rubinsztein-Dunlop, and T. W. Neely, 3, (2016).
- [35] N. Chakrova, B. Rieger, and S. Stallinga, 9330, 933008 (2015).

- [36] (n.d.) [https://www.cambridgetechnology.com/sites/default/files/Datasheet%20-%20Galvos-62xxH%20Series-DS00003\\_R1\\_v4.pdf](https://www.cambridgetechnology.com/sites/default/files/Datasheet%20-%20Galvos-62xxH%20Series-DS00003_R1_v4.pdf)
- [37] (n.d.) [https://www.thorlabs.com/newgrouppage9.cfm?objectgroup\\_id=2910&pn=CLS-SL](https://www.thorlabs.com/newgrouppage9.cfm?objectgroup_id=2910&pn=CLS-SL)
- [38] (n.d.) [https://www.nikoninstruments.com/en\\_EU/Products/Inverted-Microscopes/Eclipse-Ti-U](https://www.nikoninstruments.com/en_EU/Products/Inverted-Microscopes/Eclipse-Ti-U)
- [39] (n.d.) [https://www.nikoninstruments.com/en\\_EU/Product-Selectors/Objective-Selector](https://www.nikoninstruments.com/en_EU/Product-Selectors/Objective-Selector)
- [40] (n.d.) <https://www.thorlabs.de/drawings/f9ec036db99e8dd9-03D306A6-9987-48F4-DF653905FCBB2967/DCC1240M-Manual.pdf>
- [41] (n.d.) <https://www.thorlabs.com/drawings/445a6400ec417a63-03A187EE-0DD4-1226-9B3643961952B10E/PMM02-Manual.pdf>
- [42] (n.d.) <http://www.ti.com/tool/DLPLIGHTCRAFTER>
- [43] W. Thomas and C. Middlebrook, Opt. Photonics J. 2012, 338 (2012).
- [44] Ferrand P (2015). "GPScan.VI: A general-purpose LabVIEW program for scanning imaging or any application requiring synchronous analog voltage generation and data acquisition." Computer Physics Communications 192:342-347
- [45] (n.d.) <https://www.itl.nist.gov/div898/software/dataplot/refman2/auxillar/snr.htm>